Research Square

Preprints are preliminary reports that have not undergone peer review.
They should not be considered conclusive, used to inform clinical practice,
or referenced by the media as validated information.

Germline-targeting elicits cross-neutralizing, H3-dominated HIV CD4bs antibodies

Michael Zwick

zwick@scripps.edu

Scripps Research Institute https://orcid.org/0000-0002-0885-2502

Daniel Leaman

The Scripps Research Institute

Jinsong Zhang

Applied Biomedical Science Institute https://orcid.org/0000-0002-2195-2997

Dalton Karlinsey

Scripps Research Institute https://orcid.org/0009-0004-1786-905X

Miyo Ota

The Scripps Research Institute

Joel Allen

University of Southampton https://orcid.org/0000-0003-2547-968X

Bing Wang

Scripps Research Institute

Angel Gandarilla

Applied Biomedical Science Institute

Adam Ferguson

Scripps Research Institute https://orcid.org/0009-0003-2589-7424

Xuan Feldman

Scripps Research Institute

Mark Ochoa

Scripps Research Institute

Daniel Sands

Scripps Research Institute

Amanda Eaton

Duke University Medical Center https://orcid.org/0000-0003-3064-2947

Celia LaBranche

Duke University Department of Surgery https://orcid.org/0000-0002-6653-6655

Amanda Powell

Duke University

Christopher Cotrell

The Scripps Research Institute https://orcid.org/0000-0002-3364-3083

Daniel Ryan
Applied Biomedical Science Institute

Grace Gibson
Scripps Research Institute

Takayuki Ota
Applied Biomedical Science Institute

Agnes Walsh
The Scripps Research Institute

Mariane B. Melo
Scripps Research institute https://orcid.org/0000-0002-0409-2454

Alex LaBranche
Applied Biomedical Science Institute

Christine Shamblin
Scripps Research Institute

Spencer Brown
Scripps Research Institute

Yajing Chen
Scripps Research Institute

Armando Stano
Scripps Research Institute

Nelson Wu
Duke Human Vaccine Institute

Darrell Irvine
The Scripps Research Institute https://orcid.org/0000-0002-8637-1405

David Montefiori
Duke

Barton Haynes
Duke Human Vaccine Institute; Department of Medicine; Department of Immunology, Duke University
https://orcid.org/0000-0002-7643-9023

Max Crispin
University of Southampton https://orcid.org/0000-0002-1072-2694

Gabriel Ozorowski
Scripps Research Institute https://orcid.org/0000-0002-9695-8138

Andrew Ward
Scripps Research Institute https://orcid.org/0000-0001-7153-3769

Laurent Verkoczy
Applied Biomedical Science Institute

Article

Keywords:

Posted Date: November 19th, 2026

DOI: https://doi.org/10.21203/rs.3.rs-10073252/v1

License: This work is licensed under a Creative Commons Attribution 4.0 International License.
Read Full License

Additional Declarations: Yes there is potential Competing Interest. M.B.Z., D.P.L., L.K.V., and Scripps Research have submitted or intend to submit intellectual property disclosures and/or patent applications related to germline-targeted membrane Env liposome immunogens. D.J.I. is an inventor on a patent related to SMNP adjuvant (US11,547,672). The remaining authors declare no competing interests.

Germline-targeting elicits cross-neutralizing, H3-dominated HIV CD4bs antibodies

Authors

Daniel P. Leaman[1], Jinsong Zhang[2], Dalton C. Karlinsey[3], Miyo Ota[2], Joel D. Allen[4], Bing Wang[1], Angel Gandarilla[2], Christopher A. Cottrell[3], Adam J. Ferguson[1], Xuan Feldman[1], Mark A. Ochoa[1], Daniel I. Sands[1], Amanda Eaton[5], Celia Labranche[5], Amanda Powell[6], Daniel Ryan[2], Grace Gibson[3], Taka Ota[2], Agnes A. Walsh[1], Mariane B. Melo[1,7], Alex Labranche[2], Christine Shamblin[1], Spencer C. Brown[1], Yajing Chen[1], Armando Stano[1], Nelson R. Wu[1], Darrell J. Irvine[1,7], David C. Montefiori[5], Barton F. Haynes[6], Max Crispin[4], Gabriel Ozorowski[3], Andrew B. Ward[3], Laurent K. Verkoczy[2*], Michael B. Zwick[1*]

Affiliations

[1]Department of Immunology and Microbiology, Scripps Research Institute, La Jolla, California, USA

[2]Applied Biomedical Science Institute, San Diego, California, USA

[3]Department of Integrative Structural and Computational Biology, Scripps Research Institute, La Jolla, California, USA

[4]School of Biological Sciences, University of Southampton, Southampton, England, United Kingdom

[5]Department of Surgery, Duke University Medical Center, Durham, North Carolina, USA

[6]Duke University School of Medicine, Department of Medicine, Durham, North Carolina, USA

[7]Howard Hughes Medical Institute, Chevy Chase, MD, USA

*Correspondence: laurent.verkoczy@absinstitute.org (L.K.V.), zwick@scripps.edu (M.B.Z.)

Abstract

Eliciting broadly neutralizing antibodies (bnAbs) remains central in HIV vaccine design, yet vaccines have not induced bnAbs in humans and have had limited success in animal models. A key challenge is converting precursor B-cell recognition into maturation toward conserved epitopes on HIV Env. Here, we show that a three-shot germline-targeting regimen reproducibly activates and matures CDRH3-dominated CD4-binding-site (CD4bs) antibody precursors in CH103-lineage knock-in mice, inducing strong autologous tier-2 and selected heterologous cross-neutralizing serum responses, as well as monoclonal antibodies with tier-2 cross-neutralizing activity. This response is enabled by native-like, membrane-embedded Env arrays on liposomes bearing limited germline-targeting mutations, including the N197D glycan-site mutation, that promote B-cell activation, CH103-class somatic hypermutation, and quaternary Env-antibody recognition. Cryo-electron microscopy of representative antibodies shows recognition of a quaternary CD4bs epitope involving adjacent Env protomers, linking serum neutralization to structural maturation. Env variants that bind multiple CD4bs precursor classes further point to a membrane-Env strategy for multi-lineage germline targeting.

Introduction

An effective vaccine to prevent HIV infection remains an urgent global priority[1]. A central challenge is eliciting broadly neutralizing antibodies (bnAbs), which recognize conserved sites on the HIV envelope glycoprotein (Env) and neutralize diverse circulating viral isolates[2]. Env's dense glycan shield and sequence variability restrict antibody access, making bnAb induction difficult: lineages arise from rare germline precursors and require multiple key, often improbable, somatic hypermutations (SHM)[3, 4]. Described human HIV bnAbs have been classified into a limited set of conserved supersites on Env, with antibodies to the CD4 receptor binding site (CD4bs) among the most prominent[2]. Human CD4bs bnAbs fall into two broad classes: V_H-gene-restricted antibodies that depend on specific heavy chain genes (*e.g.*, VRC01[5]/IOMA[6] and CH235.12[7]/8ANC131[8]/1-18[9], restricted to V_H1-2 and V_H1-46, respectively) and H3-dominated antibodies that use diverse V_H genes and rely primarily on their complementarity determining region (CDR) H3 loops for epitope recognition (*e.g.*, CH103[10], VRC16, VRC13[11], and HJ16[12]).

Although human H3-dominated CD4bs bnAbs arise frequently during natural infection, vaccination strategies have not yet successfully targeted these lineages. Germline-targeting (GT) immunogens are designed to bind bnAb precursors or unmutated common ancestors (UCAs), enabling induction of V_H-restricted VRC01-like precursor B cells in humans and CH235-like precursor B cells in animal models, but not yet H3-dominated CD4bs lineages[13, 14, 15, 16, 17]. Meanwhile, elicited serum neutralization titers remain limited and largely confined to sensitive HIV isolates, highlighting the need for improved boosting strategies and broader targeting of CD4bs bnAb classes[18, 19, 20, 21]. Notably, previous gp120 subunit immunization of CH103.UCA knock-in (KI) mice elicited serum neutralization restricted to unusually sensitive tier-1 viruses and minimally mutated BCRs, consistent with reported light-chain-dependent autoreactivity and impaired BCR signaling by the CH103 UCA[22]. Thus, a central question is whether antigen format can convert germline recognition into B cell activation, affinity maturation, and serum neutralization.

Because multivalent epitope display can enhance activation of low-affinity or anergy-prone bnAb precursor B cells, including MPER, V2-apex, and other Env-directed lineages[23, 24, 25, 26, 27], we leveraged membrane Env liposomes (MELs), which present full-length, trimeric, membrane-embedded Env (mEnv) in a multivalent format amenable to germline-targeting design[21]. Native

mEnv better preserves the trimeric spike context than soluble gp120 or soluble trimer formats, while MELs add high-valency display that may improve engagement of low-affinity or tolerance-constrained bnAb precursors. We identified CH505.N197D as a minimally engineered, founder Env-derived GT mEnv variant that disrupts the N197 N-linked glycosylation (NLG) site, enabling rapid trimer recognition and cognate MEL activation of anergy-prone CH103.UCA precursor B cells.

Using this GT MEL as a prime in a short sequential regimen, we here demonstrate activation of an H3-dominated CD4bs lineage, promoting its early affinity maturation to trimeric mEnv, and induction of CH103-associated serum cross-neutralization of selected tier 2 HIV isolates. Antibody repertoire and structural analyses linked vaccine-induced SHM to neutralization breadth and recognition of an auxiliary quaternary site shared by naturally occurring bnAbs. We further identified mEnvs that engage germline precursors from multiple CD4bs lineages, supporting multivalent GT mEnv presentation as a strategy to address key immunological and structural barriers to CD4bs bnAb induction.

Results

Membrane Env liposomes convert CH103 precursor engagement into tier 2 serum neutralization

To test whether a hard-to-activate human H3-dominated CD4bs precursor could be recruited into a neutralizing response, we screened CD4bs-proximal CH505 Env variants to identify a precise germline entry point for the CH103 UCA. We screened mutants of the transmitted-founder Env, CH505.TF, carrying CD4bs-proximal N-linked glycosylation (NLG) substitutions by staining stably transduced cell lines with the CH103 lineage precursor (**Fig. 1a**). This screen identified a germline-targeting Env carrying a single NLG mutation, N197D, that enabled robust recognition of CH505 Env by CH103.UCA (**Fig. 1b**). CH103.UCA also bound purified, glutaraldehyde (GA)-fixed CH505.N197D trimeric membrane Env (mEnv) and neutralized the cognate pseudovirus, whereas no binding or neutralization was observed for CH505.TF (**Fig. 1c-d**). The N197D pseudovirus remained resistant to non-neutralizing antibodies (non-nAbs), indicating that the mutation selectively exposed the CH103 epitope while maintaining an otherwise neutralization-resistant (tier-2) Env. Further screening of CH505 variants for neutralization by CH103.UCA identified a mutant, CH505.N197D.N279D.V281A (termed N197D.m11), that was an order of magnitude more sensitive to CH103.UCA than CH505 containing N197D alone (**Extended Data Table 1**).

To investigate the role of Env glycosylation in the mechanism of CH103 UCA binding to CH505.N197D, we used mass spectrometry to compare site-specific N-linked glycan occupancy and composition between CH505.TF, CH505.N197D, and soluble Env CH505.N197D.SOS. The latter is comprised of gp120 from CH505.N197D, gp41 from BG505, “SOS” disulfide bond[28, 29], Gly-Ser rich $(GGGS)_2$ “UFO” linker in the gp41 HR1 region[30], and a stop codon at position 682. Glycosylation patterns across all three mEnvs were similar to described Envs, *e.g.* BG505, being dominated by oligomannose-type glycans (**Extended Data Fig. 1a-b, Supplementary Table 1**). Oligomannose glycans at N160 and N262 are consistent with native-like trimer folding[31]. Most NLG sites were highly occupied, except for low occupancy at N334 and N339 in the full-length mEnvs, whereas soluble CH505.N197D.SOS showed high occupancy at these sites, but minimal occupancy at N187. Notably, N276 glycans on CH505.N197D mEnv were exclusively hybrid-type rather than oligomannose, suggesting increased processing near the

CD4bs after removal of the N197 glycan (**Fig. 1e**). In contrast, CH505.N197D.SOS contained primarily $Man_5GlcNAc_2$ oligomannose-type glycans at N276, similar to other stabilized soluble Env trimers[32, 33]. Additional site-specific differences in glycan occupancy and composition were observed among the three Envs (Extended Data Fig. 1a-b). Because these differences varied by glycosylation site and several positions could not be fully resolved, they did not indicate a simple global shift in glycan processing among the constructs.

For the purpose of immunization, we incorporated purified, GA-crosslinked trimeric mEnv into multimeric membrane Env liposomes (MELs)[25], a platform designed to promote early affinity maturation against native Env. GA crosslinking was used to prevent mEnv dissociation during PGT151-purification. Env spikes and MELs were validated by antigenic, biochemical and structural analyses, using ELISA, blue native (BN)-PAGE, glycan mass spectrometry, BLI and negative stain electron microscopy (nsEM) (**Extended Data Fig. 1a-b, 2a-d; Supplementary Table 1**). GT CH505.N197D and CH505.N197D.m11 MELs were confirmed to activate CH103.UCA B cells *in vitro* (**Fig. 1f**).

Prior CH505 gp120 monomer immunization of CH103.UCA dKI mice failed to elicit detectable CH505.TF serum neutralization[22]. We designed our initial immunization studies (MEL01 and 02) to determine whether multimeric MEL immunization could overcome endogenous repertoire competition in the heterozygous double knock-in (het dKI) system and might be more effective in activating CH103 UCA B cells, because antigen multimerization has been shown to "re-awaken" anergic B cells, *e.g.* 3BNC60 and 2F5 B cells[23, 24]. MELs were formulated in CpG-ODN, Alum, and MPLA (C/A/M), an adjuvant mixture we used previously[25]. Immunization groups received adjuvant alone (Grp1), CH505.N197D virus-like particles (VLPs; Grp2), soluble CH505.N197D.SOS (Grp3), repeated CH505.N197D MELs (Grp4), or a CH505.N197D MEL prime followed by JRFL.TD15[25, 34, 35] and ADA.CM[36] MEL boosts (Grp5; **Fig. 2a**). JRFL.TD15 was selected as a CH103-sensitive first boost (IC_{50} = 0.0002 μg/ml) and ADA.CM as a more resistant second boost (IC_{50} = 0.2 μg/ml). Despite lacking transmembrane and C-terminal tail domains, our soluble Env CH505.N197D.SOS associated with liposomes likely due to the lipophilic MPER (**Extended Data Fig. 2c**).

CH103.UCA het dKI mice were generated by backcrossing homozygous CH103.UCA dKI mice to BALB/c (Study MEL01) or C57BL/6 (Study MEL02), yielding a stringent semi-polyclonal

model in which paired CH103.UCA HC/LC B cells represent only ~2% of naïve mature follicular B cells. In our early studies, BALB/c het dKI mice produced more potent serum neutralization than C57BL/6 het dKI mice, possibly due to enhanced T cell help that the H-2^d haplotype reportedly provides and/or the Th_2-skewed milieu of BALB/c relative to the C57BL/6 strain[37, 38, 39], and hence BALB/c het dKIs were used for subsequent studies (**Fig. 2a-b**).

Under matched immunization schedules, CH505.N197D MELs elicited the most potent and consistent autologous neutralization of CH505.N197D virus (mean ID_{50} ≈ 1:22,513), exceeding responses elicited by soluble CH505.N197D.SOS trimers (mean ID_{50} ≈ 1:6,496) and low-Env-copy VLPs (mean ID_{50} ≈ 1:112) (**Fig. 2b; Extended Data Fig. 3a**). Thus, among the formats tested, MEL-based multivalent presentation of membrane-embedded Env elicited the highest neutralization titers, consistent with more efficient activation of low BCR density germline precursors. Repeated immunization with CH505.N197D MELs reproducibly elicited potent autologous neutralization albeit limited heterologous tier-2 activity (**Fig. 2c; Extended Data Fig. 3a**). In contrast, sequential MEL boosting expanded neutralization to additional tier-2 isolates, including JRFL and the N197 glycan-restored virus CH505.TF, albeit with reduced titers against the GT virus. These results indicate that GT priming establishes strong autologous responses, whereas exposure to antigenically distinct Envs promotes broader heterologous recognition.

We next optimized the regimen in a follow-up study (MEL03) using second-generation CH505.N197D.m11 GT MELs (Grp8-10), escalating-dose (ED) priming[40] (Grp9-10), and the particulate SMNP adjuvant[41] (Grp10) (**Fig. 2d**). The boosting scheme was fixed to match the sequential immunization in MEL01 Grp5 *(i.e.*, JRFL.TD15 → ADA.CM MELs).

The optimized regimen in Group 10 elicited neutralization of tier-2 CH505.TF and JRFL in all immunized animals, with additional heterologous neutralization of tier-2 isolates HT593 and JR-CSF in a subset of mice (**Fig. 2e; Extended Data Fig. 3b**). ED priming also produced strong neutralization of autologous CH505.N197D virus shortly after a single immunization with CH505.N197D.m11 MELs (ID_{50} >1:1,000), whereas bolus delivery did not, and SMNP further increased neutralization titers relative to CpG/Alum/MPLA (C/A/M) (mean ID_{50} = 1:13,685 vs 1:2,230) (**Fig. 2f**). A control group (Grp6), primed with CH505.TF which did not activate CH103.UCA B cells, did not elicit any neutralization (**Fig. 2e**). Overall, these serum responses represent the strongest neutralization yet reported for a CDRH3-dominated CD4bs bnAb knock-

in model, demonstrating that sequential MEL immunization can reproducibly drive tier-2 neutralization in this stringent system.

Sera from MEL03 Groups 9 and 10, which consistently neutralized CH505.TF and JRFL, bound strongly to the CH505.gp120-core antigen (**Extended Data Fig. 4a**). We next tested the sera for binding to a CH505.gp120-core partial knockout (pKO) that eliminates mature CH103 binding (S365K, T455E, G459E), as well as a full knockout (fKO) designed to abrogate binding by most CD4bs antibodies (D368R, E370A)[42]. Serum binding was reduced by an average of 50-fold to gp120-core-pKO, with an even greater reduction for the fKO. In contrast, sera from non-neutralizing Group 6 showed ~70-fold lower binding to gp120-core than sera from Groups 9-10 with no reduction in binding to pKO. In competition ELISAs, Group 10 sera blocked binding of mature CH103 (CH103.mat) to full-length membrane Env, but not that of the V2-apex bnAb PGDM1400 (**Extended Data Fig. 4b**). Furthermore, depletion of Group 9 and 10 sera with CH505.gp120-core reduced neutralization of CH505.TF, JRFL, JRCSF, and HT593 by 5-10-fold, while depletion with CH505.gp120-core-fKO had no effect (**Fig. 2g**). Together, these results demonstrate that MEL immunization elicited potent CD4bs-directed serum neutralizing antibodies in CH103.UCA het dKI mice.

We next conducted a separate immunization study (MEL04) to assess early GC responses under SMNP/ED-priming conditions. Compared with C/A/M-adjuvanted immunization, ED/SMNP priming increased the frequency of CH505.gp120-core-binding GC B cells in draining lymph nodes, which comprised approximately 1% of the GC population, distinct from the total GC response of 20% (**Fig. 2h-i**). These responses were accompanied by increased gp120-core serum binding and a trend toward increased neutralization (**Extended Data Fig. 4c-d**). Thus, ED/SMNP priming enhanced early CD4bs-specific GC and serum responses. Although the lineage identity and HC/LC pairing of these GC B cells were not determined, all antibodies recovered by CH505.gp120-core-based B-cell sorting in study MEL03 belonged to the CH103 lineage (see below).

MEL immunization selects CH103-class B cells with cross-neutralizing somatic mutations

To define antibody lineages associated with serum neutralization, we isolated and characterized antigen-binding and lineage-relevant antibodies from CH103.UCA het dKI mice following MEL

immunization. Single B cells were sorted from the spleen and draining lymph nodes of mice from study MEL03 that showed the most potent and broad serum neutralization for high binding to a cocktail of tetramer baits including gp140 trimers from isolates CH505, JRFL, and BG505, as well as CH505.gp120-core, and low binding to CD4bs epitope knockout gp120-core-pKO (**Supplementary Table 2-3**). Using LibraSeq[43], we obtained an enriched panel of 51 unique paired CH103-lineage heavy- and light-chain sequences (**Supplementary Table 4**). No mouse or human-mouse hybrid antibodies were identified following B cell sorting.

Seven of the 51 CH103-class sequences were expressed as recombinant IgG; four of these contained SHM at positions predicted to contact Env and showed homology to CH103.mat (10X-28, 10X-23, 10X-32, and 10X-34), while three were predicted from the LibraSeq data to bind to CH505.gp120-core and not to core-pKO (10X-13, 10X-25, and 10X-39) (**Supplementary Table 3**). Three additional mAbs, sc-1-3, were isolated by conventional single-cell sorting from sequentially immunized mice in a separate immunization experiment (data not shown). All ten monoclonal antibodies (mAbs) neutralized CH505.N197D virus, eight neutralized CH505.TF, and three neutralized JRFL (**Fig. 3a**). One mAb, 10X-32, neutralized both CH505.TF and JRFL, as well as weakly neutralized the heterologous isolate JRCSF. All ten bound to varying degrees to CH505.gp120-core in ELISA (**Fig. 3b**), while two mAbs, 10X-39 and sc-3, notably cross-reacted with gp120-core-pKO, revealing a binding mode distinct from CH103.mat. However, binding by all mAbs was abrogated by CD4bs knock-out mutations D368R and E370A (CH505.gp120-core-fKO).

Across the 51 paired sequences, antibodies contained 3-15 HC and 0-10 LC SHM, with up to 8 and 4 SHM shared with CH103.mat in the HC and LC, respectively (**Fig. 3d**). Several recurrent SHM mapped to gp120-contacting positions, including K75E, S83G, and S56E/Y (**Fig. 3c**), the latter predicted to arise with low probability[44] but repeatedly selected. Reported structures of CH103 bound to gp120 and Env trimers indicate that E/Y56 contacts the gp120 CD4-binding site[10, 45, 46], whereas K75E mediates a quaternary interaction with the adjacent gp120 protomer[45]. The mAbs capable of neutralizing JRFL contained more SHM on average than those that did not and frequently carried mutations at positions implicated in Env contact, including HC-S56Y and LC-N66K (**Fig. 3e**).

To more deeply analyze CH103 lineage development post-immunization, we performed bulk Ig repertoire sequencing on splenocytes from CH103.UCA dKI mice from study MEL01 (**Fig. 2a-c**). Heavy- and light-chain transcripts from multiple isotypes were sequenced from representative mice across immunization groups. All antigen-immunized groups exhibited higher SHM rates than the adjuvant control group, with MEL-immunized mice showing more non-synonymous mutations than the VLP-immunized group, consistent with their superior neutralization responses (**Fig. 4a-b, Extended Data Fig. 5a-e**). Notably, MEL immunization, particularly sequential immunization, strongly selected for SHM at positions Q39, S54, S56, and K75, as well as other residues known to contact gp120 in CH103.mat (**Extended Data Fig. 5c**). For example, S56Y, which enhances gp120 affinity[47] but is predicted to arise infrequently, was highly enriched, particularly in sequentially immunized mice. Mutations at residue Q39, which reportedly alters heavy- and light-chain orientation to facilitate CD4bs access[48], were also common. These results show that MEL immunization reproducibly drives SHM trajectories convergent with those observed in the human CH103 lineage.

To assess how elicited HC and LC maturation patterns combine to confer neutralization, we generated recombinant mAb reassortants from bulk Ig NGS data representing diverse SHM patterns and lineage abundances (**Supplementary Table 5**). Because native HC/LC pairings are not established by bulk Ig NGS, these antibodies represent reconstructions for evaluating the functional effects of vaccine-associated SHM rather than necessarily corresponding to antibodies elicited in vivo. Thirty elicited HCs (eH) were paired with CH103 mature (mL) or germline/UCA (gL) LCs, and 11 elicited LCs (eL) were paired with CH103.mat HC (mH), enabling comparison of elicited and human-lineage SHM combinations. All mHeL mAbs neutralized CH505.TF and five cross-neutralized JRFL (**Fig. 4c; Supplementary Table 6**). Heavy chains paired with mature CH103 light chain frequently neutralized both CH505.TF and JRFL (40% of mAbs). Four mAbs also neutralized BG505 and exhibited similar SHM patterns.

Pairing the elicited HCs with the UCA light chain enhanced potency against CH505.TF virus (mean IC_{50}: 0.78 μg/ml for eHgL mAbs vs. 8.46 μg/ml for eHmL) but reduced breadth, as only 20% neutralized JRFL and none neutralized BG505 (**Fig. 4f**). This trade-off between breadth and strain-specific potency was also observed with the human CH103 chimera, CH103.mHgL, which was an order of magnitude more potent against CH505.TF than CH103.mat but showed no activity against non-CH505 viruses (**Fig. 4c**). Thus, LC SHM observed in both immunized

mice and in the original human donor promote neutralization breadth but reduce autologous neutralization of CH505.TF.

Comparison of elicited and human lineage sequences identified specific SHM associated with neutralization breadth. For example, HC position Q39[48] was frequently mutated to Leu or Arg, and Q39R associated with more frequent and potent neutralization of JRFL (**Fig. 4d**). Mutations at position 56 in CDRH2 also distinguished neutralization profiles: Y56 was strongly associated with JRFL neutralization, whereas E56 supported neutralization of CH505.TF. HC substitutions V71I and V71L and LC mutations L46V and N66K, were also associated with heterologous neutralization, with the latter two also present in CH103.mat. Strikingly, a subset of heavy chains containing a series of SHM in the CDRH2 shared with CH103.mat ([52]-YYSGS-[56] in CH103.UCA versus [52]-FHTGE-[56] in CH103 mature and H8-11) conferred neutralization of BG505 when paired with CH103 mL and were also the most potent against CH505.TF but did not neutralize JRFL (**Fig. 4e**). These results indicate acquisition of key breadth-associated features in the CH103 lineage following immunization.

We next paired L8, the most potent cross-neutralizing elicited light chain among the mHeL mAbs, with H8, the most potent elicited heavy chain among eHmL mAbs that neutralized BG505, and H17, which supported strong neutralization of both CH505.TF and JRFL when paired with both mL and gL (**Fig. 4g**). These reassortants, comprising V_H and V_L sequences recovered from the same animal, H8L8 and H17L8, each neutralized approximately half of a 12-member panel of CH103-sensitive viruses while targeting somewhat distinct subsets.

Together, these selected mAb analyses show that MEL immunization can elicit CH103-class antibodies with lineage-relevant Env-contacting mutations and cross-neutralizing activity against multiple HIV primary isolates. They further suggest that distinct heavy-chain maturation trajectories can generate complementary breadth from a common light chain.

Recurrent CH103-lineage CDRH2 insertion variants alter gp120-core recognition

We repeatedly observed CDRH2 insertions in Ig repertoire sequences from six of nine MEL-immunized het dKI mice, but not in adjuvant-only or VLP-immunized mice. These insertions occurred at low frequencies (0.000065-0.003% of sequences) and appeared to duplicate the

CH103.UCA CDRH2 motif, ^{50}YIYYSG^{55}. Three representative insertion-containing heavy chains identified by repertoire sequencing were paired with CH103 mature or UCA light chains and expressed as IgGs (H31-H33; **Extended Data Fig. 6a-c**). A natively paired mAb isolated by single B-cell sorting in a separate study (data not shown), sc-4, also contained a CDRH2 insertion.

Three of four CDRH2 insertion-containing mAbs neutralized CH505.N197D and weakly neutralized CH505.TF (IC_{50} = 34-40 μg/ml), but none neutralized JRFL or BG505 (**Extended Data Fig. 6a**). In ELISA, sc-4 and H32 bound CH505.gp120-core slightly better than or comparably to CH103.mat (**Extended Data Fig. 6b**). Moreover, when paired with the UCA LC, but not the mature LC, three of four insertion-containing mAbs retained binding to CH505.gp120-core.pKO, which contains canonical CD4bs mutations that abrogate CH103.mat binding. Thus, recurrent CDRH2 insertions define an alternative CH103-lineage maturation pattern that preserves CH505 core recognition and partially bypasses canonical CH103 knockout sensitivity, although its relevance to human antibody maturation and contribution to serum neutralization breadth remain unresolved.

Cryo-EM reveals how vaccine-selected mutations create quaternary CD4bs recognition

To define how vaccine-selected CH103-class mutations can support cross-neutralization, we determined a high-resolution (3.6 Å) cryo-EM structure of reassortant Fab H17L8 in complex with the full-length JRFL.TD15 mEnv trimer (**Fig. 5a**). JRFL.TD15 was chosen based on its higher binding affinity for H17L8 compared to CH505.N197D.m11 (K_D = 20.3 nM and 363 nM, respectively) despite similar neutralization potency (**Extended Data Fig. 2d**).

H17L8 binds to the CD4bs of JRFL.TD15 in a nested opening surrounded by glycans N188, N276, N362, and N386, while contacting the CD4 binding loop, V5, and GDMR loop (a.a. 473-476) (**Fig. 5b; Extended Data Table 2**). Notably, H17L8 makes quaternary interactions with conserved residues on an adjacent gp120 subunit, including a salt bridge between the SHM-derived D76 and K207, hydrogen bonding of E75 to S306 or Y318, and a salt bridge from the germline-encoded D72 to R308 on the adjacent protomer (**Fig. 5c-d**). Moreover, asymmetry in Fab-protomer interactions around the trimer suggests a somewhat dynamic binding mechanism. These interactions were also observed in CH103.mat (see below) and are consistent with

selection of electrostatic attractions between CH103 and the adjacent gp120 during antibody evolution (**Extended Data Table 2**); a recently published structure of CH103 in complex with Env reported similar quaternary interactions[45]. This is further supported by the observation that the germline-encoded positively charged K75 is mutated to negatively charged D or E in 61% of sequences from the mouse from which H17 was isolated (**Extended Data Fig. 5c**).

Light chain SHM in H17L8 contribute to HIV Env recognition by several mechanisms. The N66K mutation stabilizes the interface between the light chain (CDRL1 and CDRL2) and gp120 (V5 and N362/363 glycans) by hydrogen bonding with the backbone of CDRL1 G29 and V5 residue I460, while additional substitutions facilitate accommodation of conserved glycans at N276, N362, and N386 (**Fig. 5e, 6a**). Structural features of SHM in the H17L8 HC may also contribute to HIV cross-neutralization. For example, K75E and S83R form electrostatic interactions with conserved residues S306/R308 and D185, respectively, and S56Y increases buried surface area with the CD4 binding loop residue, P369 (note this residue is L369 in CH505) (**Fig. 6a**). Despite having less breadth than CH103.mat, H17L8's Y56 may be more accommodating to the 369L/P polymorphism than E56 in CH103.mat, as the aromatic ring likely can form hydrophobic interactions with either side chain, whereas the cyclic nature of Pro removes the backbone hydrogen bond donor present in the interaction between E56 and the backbone of L369 in gp120.

To compare this vaccine-selected binding mode with mature CH103, we also determined a 2.8 Å structure of CH103.mat in complex with a chimeric CH505wk4/BG505 SOSIP trimer, termed CH505wk4.c, and obtained additional negative stain EM reconstructions, all of which showed a similar binding mode (**Fig. 5f-g, Extended Data Fig. 7**; cryo-EM data collection statistics in **Supplementary Table 7** and **Supplementary Fig. 1**, sequences of structural constructs in **Supplementary Table 8**). H17L8 aligns well with the CH103.mat structure, showing a slight rotation in the light chains when aligned to gp120 (**Fig. 5g, Fig. 6a and c**). Of note, CH505wk4.c lacks the N362/363 glycan near CDRL1, which could influence the binding interface, but contains the N197 glycan that is naturally absent in JRFL.

Overall, these structures show how vaccine-selected CH103-class mutations can support cross-neutralization by accommodating conserved glycans, stabilizing antibody-Env interfaces, and enabling quaternary interactions with the adjacent gp120 protomer. Several mutations enriched

in the elicited repertoire, including K75E, S56Y, and N66K, directly contribute to these interactions, linking vaccine-selected SHM to a structural mechanism of Env recognition.

Limited somatic mutation is sufficient for selected tier 2 neutralization

To identify CH103 SHM that contribute to neutralization of selected tier-2 isolates, we first tested mature CH103 variants containing targeted germline reversions and additional substitutions selected from immunized animals or CH103-Env structural analyses. Germline reversions at positions implicated in Env recognition (G31S, ^{52}FHT^{54}→YYS, E56S, E75K and D76N) and elicited substitutions observed in CH103-lineage antibodies (E56Y and V71I/L) were tested against CH505.TF, JRFL and BG505. Reversion of FRH3 SHM E75K and D76N reduced neutralization potency by at least tenfold against all three viruses, supporting a central role for these residues in quaternary Env engagement and breadth (**Extended Data Fig. 8a**). Other substitutions had strain-specific effects: E56S reduced BG505 neutralization, whereas E56Y enhanced JRFL neutralization, consistent with structural evidence that this residue accommodates CD4-binding-loop variation[10, 48].

We next designed minimally mutated CH103 variants, termed the CH103.min series, to determine how few SHM are sufficient for neutralization of primary isolates CH505.TF and JRFL. Two mutations, HC K75E and LC L46V, generated CH103.min1, which increased CH505.N197D potency by approximately three orders of magnitude relative to CH103.UCA and enabled CH505.TF neutralization (**Fig. 7a; Extended Data Fig. 8b**). Adding adjacent-protomer contact SHM K75E and N76D to a variant containing gp120-core contact SHM[10], yielded CH103.min5, which neutralized JRFL and CH505.N197D but not CH505.TF. A light-chain-only variant containing K27R, S52W and S93R (CH103.min8) neutralized CH505.TF. Pairing this light chain with a heavy chain containing Q39L, S56Y, K75E and N76D generated CH103.min9, which neutralized both CH505.TF and JRFL, whereas reducing the heavy chain to S56Y and K75E generated CH103.min11, which decreased CH505.TF potency but increased JRFL neutralization. Finally, CH103.min15 combined LC K27R/S52W/S93R with the principal cryo-EM-defined heavy-chain contact SHM and exhibited potent neutralization of both isolates. Together, these data show that limited SHM can confer neutralization of autologous CH505.TF and heterologous JRFL viruses from a CH103.UCA precursor.

To investigate how minimal CH103 mutations confer CH505.TF-specific, JRFL-specific or cross-neutralizing activity, we generated AlphaFold3 models[49] of selected CH103.min Fvs and aligned them to experimentally determined CH103-class antibody-Env complexes. These comparisons highlighted isolate-specific constraints, although AlphaFold3's limited accuracy in modeling antibody CDR loops means these models identify potential rather than definitive interactions. In CH103-bound CH505wk4.c, CH103 displaces the N197 glycan, whereas in unbound BG505 DS-SOSIP this glycan occupies a position predicted to clash with CH103-class antibodies (**Fig. 6b**). Early CH103 intermediates may therefore require SHM that strengthen CD4bs protein contacts to overcome N197 glycan occlusion on CH505.TF, a barrier absent from JRFL. Conversely, JRFL contains an N362 glycan absent from CH505 and has a longer V5 region. AF3 models placed CH103.min L-CDR1 residues near the JRFL N362 glycan, suggesting that mutations affecting local charge or loop topology may tune glycan accommodation (**Fig. 7b**). The models also positioned LC S52W near the longer JRFL V5 loop, providing a possible basis for isolate-dependent effects on CH505 versus JRFL neutralization (**Fig. 7c**). Thus, minimal CH103 SHM preserve the H3-dominated CD4bs binding mode while tuning light-chain compatibility with isolate-specific glycan and V5-loop features.

We next asked whether neutralization (IC_{50}) correlated with Env binding (EC_{50}) by ELISA. Across CH103.min antibodies and elicited paired mAbs H17L8, H8L8, 10X-32, 10X-34 and sc-3, CH505.N197D neutralization correlated with binding to both CH505.N197D mEnv and CH505 gp120-core (**Fig. 7d**). However, broader antibodies, including H17L8 and 10X-32, bound poorly to gp120-core but efficiently recognized trimeric mEnv. Thus, mEnv binding captures quaternary determinants of neutralization not represented by gp120-core.

Related Env designs broaden H3-dominated CD4bs precursor targeting

We next asked whether this strategy could extend beyond a single CH103.UCA by testing two sources of generalizability: sequence variation among CH103-like germline antibodies and recognition of related GT Env designs by other CD4bs bnAb precursors. Glycine scanning showed that CH103 CDRH3 tolerates substantial sequence variation: all variants neutralized CH505.N197D, most neutralized CH505.TF and a subset cross-neutralized JRFL (**Fig. 7e**). Previously described CH103 V_H homologues from the same donor, IZ95W and 02IV4[10], also retained Env binding when paired with germline CH103 light chain, following the same Env-

binding hierarchy observed for CH103.UCA (**Extended Data Fig. 8f**). However, unlike CH103.UCA, these homologues did not bind monomeric CH505 gp120-core or neutralize CH505.N197D, but the single SHM K75E conferred potent CH505.N197D neutralization (**Fig. 7a; Extended Data Fig. 8f**). Thus, multiple CH103-like germline variants are preferentially engaged by trimeric GT Env and have the potential to develop neutralizing capability.

We further tested other CD4bs bnAb precursors, including both VH-restricted and H3-dominated. As previously reported, the V_H-restricted CH235.UCA bound CH505 Envs containing N279K and/or G458Y when produced under conditions that enrich Man5 glycans, such as GnTI$^-$ cells (**Extended Data Fig. 8f**)[19, 50]. Although G458Y impaired CH103 binding, both CH103.UCA and CH235.UCA recognized CH505.N197D.N279K.GnTI$^-$ Env in ELISA and neutralization assays (**Extended Data Fig. 8c,f**), and both bound purified CH505.N197D.N279K.G458Y.GnTI$^-$ mEnv (**Fig. 7f**). VRC16 is an H3-dominated CD4bs bnAb with a CH103-like footprint but no CH103 sequence homology[11]. Fully germline-reverted VRC16.gHgL did not bind or neutralize CH505.N197D or JRFL, whereas a partially reverted VRC16 construct containing four SHM (rH4:gL) neutralized both viruses and bound GA-crosslinked and purified mEnv, with a preference for CH505.N197D.m11 produced in GnTI$^-$ cells (**Fig. 7f; Extended Data Fig. 8d–f**). In contrast, inferred germline VRC13, an H3-dominated CD4bs bnAb with a distinct footprint, did not neutralize CH505.N197D or JRFL and did not bind the tested mEnv trimers, although it bound gp120-core antigens that were also recognized by CH103.UCA (**Fig. 7f; Extended Data Fig. 8d–f**).

Together, these results show that specifically engineered Env immunogens used to drive CH103-lineage responses can also engage precursors from multiple CD4bs bnAb lineages. Thus, optimized GT MEL immunization can activate and mature CH103-lineage B cells toward quaternary Env recognition and cross-neutralizing activity, while related Env designs conditionally engage CH235-, VRC16- and VRC13-like precursors.

Discussion

This work extends CD4bs germline targeting beyond V_H-restricted antibody classes. Most CD4bs GT strategies have focused on V_H-restricted classes such as VRC01, IOMA, and CH235, yet induction of broadly neutralizing responses in humans remains elusive, and single-lineage targeting may be insufficient for protection[11, 51, 52, 53]. Here, full-length membrane-embedded GT Env displayed on MELs efficiently activated and matured the CH103 class, expanding bnAb germline-targeting space to include H3-dominated CD4bs lineages. Vaccination recapitulated key features of CH103 lineage evolution, including SHM that contact quaternary Env surfaces, while eliciting CH103-associated tier-2 cross-neutralizing serum responses.

MELs outperformed the VLP and soluble Env formats tested, eliciting more potent and reproducible serum cross-neutralization and stronger CH103-class SHM in memory B-cell repertoires. This likely reflects the combined effects of higher Env density, reduced off-target antigen display, and native membrane-embedded trimer presentation. Full-length mEnv also preserves MPER and other epitopes absent or altered in many soluble Env designs, providing a platform for co-targeting additional bnAb specificities. Structural analyses further highlighted the importance of native trimer recognition, identifying E75 as an early, dominant CH103 HC SHM that enables trimer binding and neutralization by forming quaternary contacts with a neighboring gp120 protomer, with D76 contributing to the same interface[45]. This adjacent region, CD4bs2, is also engaged by CD4 and several potent bnAbs, supporting inter-protomer recognition as a recurring structural feature of broadly neutralizing CD4bs responses[54]. Recent heterologous trimer immunization studies in nonhuman primates elicited the LJF-0034 bnAb lineage, which recognizes a distinct quaternary gp120:gp120 interface epitope with light-chain contacts in the CD4bs and heavy-chain contacts in V3 and conserved V2 elements.

Precise glycan remodeling at N197 proved critical. CH505.N197D was sensitive to CH103.UCA neutralization, whereas some alternative substitutions (**Extended Data Table 1**) or broader removal of other CD4bs-proximal glycans[50] were not, indicating that CH103.UCA engagement is site-selective rather than a consequence of global glycan reduction, and depends on both loss of the N197 glycan sequon and local side-chain chemistry. Thus, minimally engineered mEnv

trimers can create germline entry points while preserving the native antigenic architecture needed for maturation.

Neutralization of selected primary isolates required relatively few SHM, and activity retained by CH103 CDRH3 variants and heavy-chain homologues revealed substantial sequence tolerance within the lineage. Recurrent CDRH2 insertions further suggest plasticity in CH103-class maturation, paralleling prior computational CH103 redesign in which H2-loop extension improved gp120 binding[47]. Because CH103 uses a normal-length CDRH3 and related precursors occur at measurable frequencies in humans[10], H3-dominated CD4bs responses represent plausible vaccine targets.

Although the CH103.UCA het dKI model does not reproduce a fully outbred Ig repertoire, it allows human CH103 precursors to mature in competition with predominantly endogenous B cells. Thus, the het dKI model is suited to direct study of the CH103 lineage and can inform studies of analogous HCDR3-dominated responses in macaques with an outbred repertoire. Engineered CH505 variants further engaged multiple CD4bs precursor classes, including fully or partially germline-reverted CH235, VRC16, and VRC13, consistent also with the co-occurrence of V_H-restricted and H3-dominated CD4bs bnAb lineages in single donors[10, 11]. These data support multi-lineage GT strategies designed to engage complementary precursor repertoires, although activation and maturation of additional lineages will require direct testing.

An escalating-dose SMNP regimen has been reported to enhance activation and maturation of rare bnAb precursors[55, 56] and here also increased serum responses to the current H3-dominated CD4bs target, consistent with a role for sustained germinal center engagement[56]. CH103.UCA anergy reflects a physiological B-cell tolerance mechanism, and the recruitment of such low-responsive precursors suggests that appropriately adjuvanted, multivalent GT vaccination regimens can overcome this barrier. Although MELs have not yet been clinically evaluated, their transmembrane Env display in a saponin-based particulate formulation resembles a clinically validated SARS-CoV-2 spike vaccine platform[57]. Recent HVTN300 clinical data identifying CH505-induced CD4bs-overlapping CDRH3-binder precursor responses in human vaccinees[58], together with glycan-deleted SHIV-CH505 bnAb induction in macaques[59, 60], support CH505-based immunization to elicit CD4bs bnAbs, although maturation toward the breadth of the mature CH103 remains a key unmet challenge.

The genetic and structural diversity of CD4bs bnAbs suggests that targeting multiple antibody lineages could reduce dependence on individual precursor classes and improve coverage across human repertoires. The HIV CD4bs forms a glycan-gated surface spanning adjacent Env protomers that allows distinct antibody lineages to converge on a shared conserved interface, yet native Envs typically fail to engage their precursors. Targeted glycan remodeling and affinity-enhancing substitutions can therefore balance enhanced germline recognition with preserving mEnv integrity. For highly variable pathogens with a single spike, including HIV-1, HCV E1E2, and Lassa GPC, vaccine strategies may need to elicit multiple bnAb specificities against the same conserved footprint to maximize breadth. Together, our findings establish H3-dominated CD4bs antibody lineages as tractable GT vaccine targets and identify minimally engineered membrane-based GT immunogens that can promote CH103-lineage maturation while providing entry points for broader multi-lineage CD4bs targeting.

Author Contributions

D.P.L, X.F., M.A.O., D.I.S., A.E., C.L., S.C.B., and A.J.F. performed binding and neutralization assays. J.Z., M.O., C.S., Y.C., and A.S. performed flow cytometry. M.O., A.G., and A.P. provided animal care, performed immunizations, and collected samples. A.A.W. and M.B.M produced SMNP adjuvant. J.Z. and M.O. carried out B cell sorting and *ex vivo* cellular analyses. J.D.A performed glycan analysis. D.C.K., C.A.C., N.R.W, G.G. and G.O. determined cryo-EM and negative stain EM structures. G.O. performed AlphaFold modeling. D.P.L., J.Z., M.O., D.R., and T.O. performed next generation sequencing. D.R. performed single-cell PCR. D.P.L., B.W., T.O., and A.L. provided bioinformatic analysis. D.J.I. provided resources. D.C.M., B.F.H., M.C., A.B.W., L.K.V., and M.B.Z. supervised research and provided funding. D.P.L, L.K.V., and M.B.Z. conceptualized experiments and prepared the manuscript with input from all authors.

Acknowledgements

This work was supported by NIH grants R01 AI152523 and AI181784 (M.B.Z.), R01 AI087202 (L.K.V.), R01 AI175489 and UM1 AI144462 (D.J.I.), and UM1 AI144371 for the Duke Consortia for HIV/AIDS Vaccine Development (B.F.H.), with initial support from P01 AI104722 (R.T. Wyatt, Scripps). Reagents used in this study were developed with support from NIH grant R01 AI183472 (M.B.Z.). The cryo-EM work was funded by Cooperative Agreement award UM1

AI144462 in partnership with the Division of AIDS, NIAID (A.B.W.) and used equipment supported by NIH grant S10OD032467. Glycan analysis was supported by the Gates foundation CAVD (INV-070116; M.C.). The James B. Pendleton Charitable Trust (M.B.Z.) enabled the purchase of crucial equipment. We thank S. Head, J. Ledesma, A. Domissy and P. Nataraja at the Scripps Genomics Core, as well as the UCSD NGS sequencing core for next generation sequencing and bioinformatics assistance. We also thank T. Fassell and S. Henderson for negative stain EM of MELs.

Data Availability

- Cryo-EM maps have been deposited in the Electron Microscopy Data Bank (EMDB; https://www.ebi.ac.uk/emdb/) under accession codes EMD-71963 and EMD-71965, and cryo-EM models have been deposited in the Protein Data Bank (PDB; https://www.rcsb.org/) under accession codes 9PXA and 9PXE. Models have been made public and PDB validation files have been uploaded with the manuscript.
- Mass spectrometry data for site-specific glycan analysis is available at massive.ucsd.edu under accession code MSV000099706. Username for web access: MSV000099706_reviewer, username for FTP access: MSV000099706, password: 4VUd5FqBrt6lJPjZ.
- The sequencing data generated in this study have been deposited in the NCBI Gene Expression Omnibus (GEO; https://www.ncbi.nlm.nih.gov/geo/query/acc.cgi) under accession codes GSE312573 (bulk NGS from MEL01; reviewer token sxazeimidfgbput) and GSE312578 (single cell sequencing from MEL03; reviewer token axcfkqcuvrabdwt).
- Code used to analyze sequencing data is deposited at https://github.com/BWANG2016/cigunpaired. Scripts used to generate 2D histograms, logoplots, phylogenetic trees, and SHM probability have been deposited at https://github.com/CH103-analysis/analysis_scripts/releases/tag/v1.0.0. All depositions have been made publicly available.

Competing interests

M.B.Z., D.P.L., L.K.V., and Scripps Research have submitted or intend to submit intellectual property disclosures and/or patent applications related to germline-targeted membrane Env

liposome immunogens. D.J.I. is an inventor on a patent related to SMNP adjuvant (US11,547,672). The remaining authors declare no competing interests.

Materials and Methods

Generation of pseudotyped HIV. HIV pseudotyped virus was produced by transient transfection of HEK293T cells using Env plasmid DNA, pSG3ΔEnv backbone plasmid, and 25 kDa PEI as transfection reagent, as previously described[61]. Virus-like particles (VLPs) for immunization were similarly prepared but were purified over an iodixanol density gradient and inactivated using Aldithiol-2 (AT-2) as previously described[62]. Env content in VLPs was quantified using a GNL-capture ELISA as compared to purified, sequence-matched Env trimers.

Recombinant protein production. Genes of interest were synthesized or generated by site-directed mutagenesis at Genscript. Antibodies and soluble Env proteins were produced by transfection of ExpiCHO cells (ThermoFisher), according to the manufacturer's instructions. On the day before transfection, cells were split at a density of 3 x 10^6/ml in 25 ml ExpiCHO medium (ThermoFisher). After 24 h, DNA (25 µg total) was added to 1 ml OptiPro SFM (ThermoFisher) and 0.2 µm filtered. Antibodies were produced by transfecting HC and LC plasmids in equal amounts; gp120-core proteins were generated using a single plasmid, while for soluble gp140s the *env* plasmid and a separate plasmid encoding furin were transfected in a 4:1 ratio. In a separate tube, 80 µl of Expifectamine (ThermoFisher) was added to 920 µl OptiPro SFM. The Expifectamine mixture was added to the DNA, incubated for 3 min, and then added dropwise to the ExpiCHO cells. The following day, 6 ml of ExpiCHO Feed and 150 µl Enhancer (ThermoFisher) were added to the cells, and they were moved to a 32°C incubator. Supernatants were harvested 6 days post-transfection and proteins were purified using either Protein A Sepharose (antibodies; ThermoFisher) or GNL agarose (Env; Vector Laboratories) according to the manufacturer's directions.

ELISA. ELISAs were performed as previously described [25]. Microtiter wells were coated with GNL (5 µg/ml) in PBS overnight at 4˚C, then purified mEnv trimers or gp120-cores (5 µg/ml) in PBS containing 0.1% DDM were captured for 2 h at 37˚C. Plates were blocked with 4% non-fat dry milk (NFDM) in PBS for 1 h at 37˚C. Primary and HRP-conjugated secondary antibody (Jackson Immunoresearch) incubations were performed at 37˚C for 1 h and 45 min, respectively, in PBS containing 0.05% Tween-20 and 0.4% NFDM. Microtiter wells were washed 4 times with PBS + 0.05% Tween-20 between each step. Following all incubations, TMB substrate (ThermoFisher) was added for 5 min, the reaction was stopped by adding 2N H_2SO_4, and absorbance was read at 450 nm.

Neutralization assays. Neutralization assays were performed using pseudotyped viruses as previously described [25]. Briefly, 96-well plates were seeded with TZM-bl cells[63] (obtained through BEI Resources, NIAID, NIH: HRP-8129) in 50 µl of Growth Media (DMEM + 10% FCS, 20 mM L-glutamine, 100 U/ml penicillin, 100 µg/ml streptomycin and 10 µg/ml DEAE-dextran) and incubated overnight at 37°C. Virus was mixed with antibody, or with serum that had been

inactivated at 56°C for 30 min; the mixture was incubated at 37°C for 1 h and then added to TZM-bl cells. Infectivity was determined 72 h later by addition of Bright-Glo luciferase reagent (Promega), according to the manufacturer's instructions, and luminescence was measured using a Synergy H1 plate reader (BioTek). In some cases, neutralization assays were similarly performed except that freshly trypsinized cells were added after the mixture of virus and serum, instead of being pre-seeded, and luminescence was read using the Britelite Luminescence Reporter Gene Assay System (PerkinElmer Life Sciences)[64].

Depletion of antibodies from serum. Biotinylated CH505.gp120-core and CH505.gp120-core-fKO were coupled to Dynabead MyOne Streptavidin T1 (ThermoFisher) beads according to the manufacturer's protocol. Beads were washed three times with 293T growth medium containing 10% FBS and blocked using the same medium for 30 min at room temperature. Serum samples, diluted 1:20, or mAbs, diluted to 20 µg/ml, were prepared in 200 µl of 293T medium for each depleting antigen. Samples were incubated with antigen-coupled beads for three consecutive rounds of 30 min each at room temperature with rotation, using fresh beads for each round. Following depletion, beads were magnetically separated and the depleted samples were collected for subsequent analysis.

Blue Native (BN)-PAGE. BN-PAGE was performed using the NativePAGE gel system (ThermoFisher), according to the manufacturer's instructions. Purified mEnv (5 µg) was suspended in the supplied sample buffer and 0.5% DDM and run on a 3-12% gradient Bis-Tris NativePAGE gel at 150 V for 3 h at 4˚C. Gels were stained using Simply Blue Safe Stain (ThermoFisher), according to the manufacturer's instructions. Gels were imaged using a Chemidoc instrument (BioRad) and bands were quantified using ImageLab software (BioRad).

Negative stain EM of liposomes. Liposomes were applied for 2 min onto glow discharged, carbon-coated 400-Cu mesh grids (Electron Microscopy Sciences). Excess sample was removed by gentle contact with tissue paper, and the grids were placed on a droplet of 2% phosphotungstic acid (PTA) solution (pH 6.9) for 2 min. Excess stain was removed and grids were examined on a Philips CM100 electron microscope (FEI) at 80 kV. Images were acquired using a Megaview III charge-coupled device (CCD) camera (Olympus Soft Imaging Solutions).

Generation of Env cell lines. Cell lines expressing CH505.N197D, JRFL.TD15, and ADA.CM.V4 were described previously[25, 65]. Cell lines expressing CH505.TF and CH505.N197D.SOS were prepared similarly using lentiviral transduction followed by iterative rounds of fluorescence-activated cell sorting (FACS) gating for a PGT145^{high} b6^{low} phenotype. The CH505.N197D.SOS Env construct is comprised of CH505 gp120 and BG505 gp41 sequences, the latter of which increases trimer stability relative to CH505.TF[66]. The glycoprotein was further stabilized by the addition of the SOS disulfide (A501C and T605C) and the UFO linker $(GGGGS)_2$ replacing residues 548-568 in HR1 of gp41. Of note, sequencing of genomic

DNA prepared from cognate cells revealed that *env* gene CH505.N197D.SOS acquired a spontaneous mutation that caused truncation of Env at amino acid position 682.

The cell line expressing CH505.N197D.m11 was generated similarly to above, except the *env* gene (including a stop codon at amino acid position 755 in the C-terminal tail) was cloned in the pLenti CMVTRE3G pDEST Puro plasmid. Lentivirus was transduced into 293T cells stably expressing rtTA3G from the pLenti CMV rtTA3G Blast vector[67]. The next day cells were selected with 2 µg/mL puromycin. Cells stably expressing the *env* gene were induced with doxycycline (1 µg/mL) and sorted using flow cytometry, as noted above.

Flow Cytometry of Env expressing cells. HEK293T cells plated at 2.5 x 10^6/ml in 2.5 ml Growth Media in 6-well plates, were transduced with lentiviral vector using the same method that was used to generate stable Env cell lines in the previous section. After 48 h, cells were washed with FACS buffer (PBS supplemented with 2% heat-inactivated FBS) and labeled with Fixable Aqua Live/Dead Cell Stain (Life Technologies) for the detection of dead cells. Cells were washed with FACS buffer and resuspended in 50 µl of FACS buffer containing primary Ab and incubated for 15 min at 4°C. Following another wash with FACS buffer, cells were resuspended in 50 µl of FITC-conjugated anti-human-Fcɣ secondary Ab (Jackson Immunoresearch) and incubated for 15 min at 4°C. Samples were washed, and at least 10,000 cells were acquired on a Novocyte flow cytometer (Agilent). Data were analyzed using FlowJo software (Tree Star). Dead cells and doublets were excluded from the analysis.

Purification of HIV membrane Env. Cell lines that overexpress mEnv were grown in shaker flasks at 37˚C in 8% CO_2 atmosphere to a density of 4 x 10^6 cells/ml, then pelleted by centrifugation at 300 x *g* for 5 min. The cell pellet was resuspended in PBS and treated with 15 mM glutaraldehyde (GA; Sigma) at room temperature (RT) for 10 min. Unreacted GA was quenched for 15 min in 50 mM Tris-HCl, after which treated cells were solubilized for 20 min in 0.5% DDM (Sigma). Cell debris was removed by centrifugation at 3000 x *g* for 15 min at 4˚C, then the supernatant was clarified by spinning at 40,000 x *g* in a Sorvall centrifuge (ThermoFisher) for 1 h at 4˚C. MEnv was affinity purified using the trimer-specific bnAb PGT151. PGT151-coupled Protein A Sepharose beads (GE Healthcare) were added to the supernatant, and the mixture was rotated overnight at 4˚C. The beads were washed with TN75 (20 mM Tris, pH 8, 500 mM NaCl, 0.1% DDM, 0.003% sodium deoxycholate) and bound mEnv was eluted in 3M $MgCl_2$. The trimer fraction was purified by size exclusion chromatography using a Superdex 200 10/300 GL column, TBS containing 0.1% DDM and 0.003% sodium deoxycholate as running buffer, and an ÄKTA Pure 25L HPLC instrument (GE Healthcare) at a flow rate of 0.75 ml/min.

Formation of membrane Env liposomes (MELs). Naked liposomes were prepared by dissolving 1-palmitoyl-2-oleoyl-glycero-3-phosphocholine (POPC) and cholesterol (Avanti) in chloroform at a 70:30 molar ratio. Lipids were dried in a vacuum overnight, hydrated in PBS (20

mg/ml total lipid) with constant shaking for 2 h at 37°C, then sonicated for 30 s. The resulting liposomes were extruded 14 times through 0.8 μm, 0.4 μm, 0.2 μm, and 0.1 μm filters using a mini-extrusion device (Avanti) at RT, then diluted to 4 mg/ml in PBS. DDM was added to a final concentration of 0.1% (1.9 mM, detergent:lipid molar ratio = 0.3:1) to destabilize the lipid bilayer. Purified mEnv trimers were added at a 1:10 trimer:lipid ratio (w/w, and final concentrations of 1.9 mM DDM and 7.2 μM sodium deoxycholate) and the mixture was incubated at RT for 15 min. To remove detergent, polystyrene Bio-beads SM2 (Bio-Rad), pre-washed once with methanol and five times with water, were added at 40 mg/ml and the sample was rotated at RT for 30 min. Liposomes were treated thrice more with fresh Bio-beads at 4°C for 1 h, overnight, and 2 h, respectively. MELs in the supernatant were drawn off the polystyrene beads using a pipette. To remove residual detergent, the volume was brought up to 15 ml by addition of PBS and MELs were concentrated again using a 100 kDa molecular weight concentrator (MilliporeSigma). The resulting MELs were stored at 4°C for up to three days or frozen in aliquots at -80°C for longer storage.

Biolayer Interferometry (BLI). *Streptavidin Capture Assay.* Binding kinetics of Fab–antigen interactions were measured using an Octet Red 384 system (FortéBio). All reagents were diluted in BLI buffer: PBS (pH 7.4) with 0.01% BSA and 0.002% Tween-20. Streptavidin (SA) biosensors (Sartorius) were pre-hydrated in buffer for ≥10 min, then equilibrated in BLI buffer for 60 s to perform a sensor check. Biotinylated antigen (7.5 μg/ml) was loaded onto SA sensors for 660 s, followed by a 300 s baseline in BLI buffer. Sensors were then transferred into a 2-fold serial dilution of Fab for 100 s (association), and subsequently into a corresponding 2-fold PBS dilution series for 900 s (dissociation). The PBS volumes matched those of the Fab solutions in the association step. Each experiment included a reference sensor (no Fab). All measurements were conducted at 25 °C with plate shaking at 1000 rpm. Sensorgrams were background-subtracted using reference data, aligned to the association step, inter-step corrected, and Savitzky-Golay filtered. Kinetic data were globally fit to a 1:1 binding model using the full association and dissociation intervals.
Streptavidin–Biotinylated Lectin Capture Assay. For Fab binding to lectin-captured glycoprotein, BLI buffer was supplemented with 0.01% DDM. SA sensors were loaded with 5 μg/ml biotinylated wheat germ agglutinin (WGA; Vector Laboratories) for 240 s, then, after a 300 s baseline in BLI buffer, transferred to 1.25 μg/ml membrane-bound Env (mEnv) for 660 s. After antigen capture, sensors were equilibrated in BLI buffer for 1800 s (baseline). Association and dissociation steps were performed as described above.

HIV Env N-linked glycosylation analysis. Uncrosslinked HIV mEnv prepared from cells was bound to PGT151 resin, as detailed above. The beads were subsequently incubated at 100˚C for 5 min in Laemli buffer containing 50 mM DTT, the beads were pelleted, and the supernatant was run on Novex 8-16% Tris Glycine SDS-PAGE gels (ThermoFisher) according to the manufacturer's instructions. Gels were stained with SimplyBlue SafeStain (ThermoFisher). Gel

bands corresponding to Env were excised, cut into small pieces, dehydrated using 100% acetonitrile, which was replaced with 100 mM ammonium bicarbonate containing 10 mM DTT and incubated for 30 min at 56˚C. A second acetonitrile wash was used to remove the DTT, before incubating with 55 mM IAA in 100 mM ammonium bicarbonate. Gel bands were destained overnight with a 50:50 mixture of acetonitrile and 100 mM ammonium bicarbonate in water. The next day, the solution was replaced with 10% acetonitrile in 100 mM ammonium bicarbonate, and either trypsin-LysC, chymotrypsin (Promega) or alpha lytic protease was added at a ratio of 1:30, or 1 µg of protease per 30 µg sample. Gel bands were incubated overnight at 37°C. Peptides and glycopeptides were extracted from the gel band by first adding acetonitrile to the protease digestion mixture (2:1 v/v), extracting and placing the supernatant into a fresh tube and then adding 1:2 v/v 5% formic acid/acetonitrile for 15 min at 37°C. The two extractions were pooled and dried down using a heated vacuum centrifuge. Peptides were extracted using C18 Zip-tip (MerckMilipore).

Eluted peptides were dried, re-suspended in 0.1% formic acid, and analyzed by nanoLC-ESI MS with an Ultimate 3000 HPLC (ThermoFisher Scientific) system coupled to an Orbitrap Eclipse mass spectrometer (ThermoFisher Scientific) using stepped higher energy collision-induced dissociation (HCD) fragmentation. Peptides were separated using an EasySpray PepMap RSLC C18 column (75 µm × 75 cm). A trapping column (PepMap 100 C18 3 µM 75 µM x 2cm) was used in line with the LC prior to separation with the analytical column. The LC conditions were as follows: 280 min linear gradient consisting of 4-32% acetonitrile in 0.1% formic acid over 260 min followed by 20 min of alternating 76% acetonitrile in 0.1% formic acid and 4% Acn in 0.1% formic acid, to ensure all the sample had eluted from the column. The flow rate was set to 300 nL/min. The spray voltage was set to 2.5 kV and the temperature of the heated capillary was set to 55°C. The ion transfer tube temperature was set to 275°C. The scan range was 375−1500 m/z. Stepped HCD collision energy was set to 15, 25 and 45% and the MS2 for each energy was combined. Precursor and fragment detection were performed using an Orbitrap at a resolution MS1= 120,000; MS2= 30,000. The AGC target for MS1 was set to standard and injection time set to auto, which involves the system setting the two parameters to maximize sensitivity while maintaining cycle time.

Glycopeptide fragmentation data were extracted from the raw file using Byos (Version 4.0; Protein Metrics Inc.). The glycopeptide fragmentation data were evaluated manually for each glycopeptide; the peptide was scored as true-positive when the correct b and y fragment ions were observed along with oxonium ions corresponding to the identified glycan. MS data were searched using the Protein Metrics 305 N-glycan library with sulfated glycans added manually. All charge states for a single glycopeptide were summed. The precursor mass tolerance was set at 4 ppm and 10 ppm for fragments. A 1% false discovery rate (FDR) was applied. The relative amounts of each glycan at each site and the unoccupied proportion were determined by comparing the extracted ion chromatographic areas for different glycopeptides with an identical peptide sequence.

Glycans were categorized according to the composition detected. HexNAc(2)Hex(10+) was defined as M9Glc, HexNAc(2)Hex(9−5) was classified as M9 to M3. Any of these structures containing a fucose were categorized as FM (fucosylated mannose). HexNAc(3)Hex(5−6)X was classified as Hybrid with HexNAc(3)Hex(5-6)Fuc(1)X classified as Fhybrid. Complex-type glycans were classified according to the number of HexNAc subunits and the presence or absence of fucosylation. As this fragmentation method does not provide linkage information, compositional isomers are grouped, so, for example, a triantennary glycan contains HexNAc 5 but so does biantennary glycans with a bisect. Core glycans refer to truncated structures smaller than M3. M9glc- M4 were classified as oligomannose-type glycans. Glycans containing at least one sialic acid, or one sulfate group were categorized as NeuAc, or sulfated, respectively.

B cell calcium flux assay. For analysis of Ca^{2+} flux induced by transient BCR-signaling, CH103 UCA dKI splenocytes were depleted of red blood cells by ACK lysis and then stained with BV650 anti-B220 (BD Cat#563893) and R718 anti-CD19 antibodies (BD Cat#567063) for 30 min. After washing with HEPES-buffered saline (HBSS), pre-stained cells were loaded with Fluo-4 via by mixing with an equal volume of Fluo-4 loading solution (Fluo-4 Direct Calcium Assay Kit, ThermoFisher, Cat# F10471) according to the manufacturer's instructions. After incubating for 30 min at 37℃ and then 30 min at RT, cells were washed with HBSS and incubated with LIVE/DEAD Near-IR for 30 minutes. Cells were washed twice with HBSS, resuspended in [Ca2+]-supplemented HBSS, incubated at RT for 5 min, and then transiently activated by treatment with various MEL immunogens or F(ab')2 anti-IgM (Southern Biotech). Raw Fluo-4 MFI data was acquired on a BD FACSCelesta flow cytometer and total live B-cell (B220+CD19+) responses were analyzed using FlowJo software.

Immunization of mice. All experiments were performed using 8-12-week-old mice. Each group had at least one female mouse. Animals were housed in the ABS vivarium under specific pathogen–free conditions, maintained on a 12-h light/dark cycle at 20–25°C, and handled in accordance with NIH and AAALAC guidelines under ABS Institutional Animal Care and Use Committee (IACUC)-approved protocols. The homozygous CH103.UCA double knock-in (dKI; $V_HDJ_H{}^{+/+}$ $V\kappa J\kappa^{+/+}$) line was generated on a C57BL/6 background. To produce CH103.UCA heterozygous F1 (het dKI F1) mice, homozygous CH103.UCA dKI mice were bred with BALB/c mice. For immunizations, CH103.UCA het dKI F1 mice were injected subcutaneously in both hind legs with 50 μg of antigen either as a bolus prime (Day 0) or an escalating dose on Days 0, 2, 4, 7, 9, 11, and 14, delivering a total of 50 μg of immunogen with each subsequent dose increased by a factor of 2.718. The C/A/M adjuvant consisted of CpG ODN1826 (20 μg/mouse; InvivoGen), monophosphoryl lipid A (MPLA; 10 μg/mouse; InvivoGen), and alum (¼ total volume; Pierce)[25]. In later experiments, SMNP (5 μg/mouse) was produced as previously described[41] and used as the adjuvant. Blood collections and booster immunizations were performed at the time points indicated in the figure legends.

Flow cytometry analysis of mouse B cells. Flow cytometric analysis of B cell development was performed as previously described[22]. Single suspensions of total splenocytes and/or draining lymph nodes were stained using 0.5 µg/ml of anti-B220 AF700 (BD cat #557957), anti-CD19 BV650 (BD cat #557957), anti-CD138 BV786 (BD cat # 569692, anti-CD38 PE (BD cat# 553764), anti-GL7 AF647 (BD cat # 561529), anti-IgM PEcy7 (BD cat #552867), anti-IgG1 BV510 (BD cat #740121), anti-IgG2a/2b BV510 (BD cat #744293), anti-IgG3 BV510 (BD cat #744134), CH505Core-PECF594 and KO-CH505Core-BV421. All Abs were obtained from BD Biosciences. Cells were washed with Dulbecco's phosphate-buffered saline (DPBS) and stained with LIVE/DEAD® Near-IR 20 min at RT. Cells were washed twice with DPBS and analyzed by BD on a BD FACSCelesta flow cytometer.

CH505.gp120-core and core-KO tetramers were produced by incubating streptavidin-PE or streptavidin-APC (BioLegend) with a four-fold molar excess of gp120-core protein for 1h on ice. CH505.gp120-core+ GC B cells were visualized by first gating on lymphocyte singlets, followed by exclusion of dead cells that stained positively using LIVE/DEAD® Near-IR staining reagent and subsequently gating for CD19+B220+ (total B cells), then CD38-GL7+ and finally, gating for CH505.gp120-core+ and CH505.gp120-core-KO- cells.

Antigen sorting of mouse B cells. Antigen binding B cells were enriched from spleen or draining lymph nodes (dLNs) harvested from immunized CH103.UCA het dKI mice. For capturing antigen specific B cells, biotinylated antigens were coupled with TotalSeq^{TM}-PE Streptavidin and Streptavidin-APC (BioLegend). To minimize sorting for non-specific binders, each antigen was labeled with both PE and APC, and double positive B cells were sorted. Briefly, total splenocytes and dLNs cells were labeled with equal amounts of PE and APC labeled antigen streptavidin tetramers and PE labeled B cells were enriched by using anti-PE microbeads (Miltenyi Biotec) following manufacturer's instructions. After enrichment, each sample of 0.5 to 1 µg/1x10^6 cells was cell hashed using TotalSeqC antibody-oligonucleotide conjugate (BioLegend). Cell-surface marker stains were performed using standard protocol with the following antibodies at 1:200 dilution in FACS buffer (HBSS containing 0.5 % BSA and 1 mM EDTA): TruStain FcX^{TM} PLUS (mouse Fc blocking solution, BioLegend), FITC anti-IgMb, PE/Dazzle 594 anti-CD19 (6D5, BioLegend), PECy7 anti-TCRbeta (H57-597, BioLegend), PECy7 anti-IgMa. H57$^-$CD19$^+$IgMa$^-$IgMb$^+$PE$^+$APC$^+$ B cells (IgM$^+$ antigen specific B cells) and H57$^-$CD19$^+$IgMa$^-$IgMb$^-$PE$^+$APC$^+$ B cell (IgM- antigen specific B cells) were sorted on a SH800S Cell Sorter (SONY). After confirming cell number and viability, B cells were run on a Chromium 10X controller using 5' chemistry (10X Genomics) in two lanes with an expected recovery rate of 10,000 cells per lane, according to the manufacturer's instructions. Libraries were generated and run on a Novaseq 6000 (Illumina).

BCR sequencing from single cells using 10X Genomics technology. BCR sequence data from 10X Genomics BCR sequencing began with the filtered V(D)J contigs from 10X Genomics Cell Ranger version 3.1. To obtain V and J gene assignments, these contigs were aligned to the

IMGT GENE-DB germline reference allele database (obtained 8/3/2019) (62). Non-productive heavy and light chain BCR sequences were removed. BCRs were annotated by B cell subtype based on matching their single cell barcodes to the gene expression information. Only cells that had both gene expression and BCR sequence data were retained. In cells with multiple heavy chains, only one heavy chain with the highest unique molecular identifier count was retained. In the event of a tie, the first heavy chain identified was retained.

BCR sequencing from single cells using PCR. Sorted B cells were deposited into individual 96-well plates and BCR cDNAs were generated by reverse transcription synthesis using SuperScript III Reverse Transcriptase and random primers as per the manufacturer's instructions (LifeTech), followed by two rounds of PCR amplification using Ig reverse and forward primer sets. For isolation of KI HC rearrangements, forward primers (outer and nested) were used that were specific for either the common J558 H10 leader peptide in the KI HC expression cassette or human V_H4-59. Likewise, for isolation of LC rearrangements, forward primers specific to either the common VκOx1 leader peptide in the KI LC expression cassette or human V_λ3-1 gene-specific were used. Cloned PCR products were then purified and directly sequenced in both orientations (GeneWiz). CH103.UCA KI V_HDJ_H and $V_\lambda J_\lambda$ KI rearrangements were sequenced in both directions and analyzed for SHM using MegAlign Pro multiple sequence alignment software (DNASTAR).

Next generation sequencing. Splenocytes from CH103 het dKI mice were removed from cell stroma into PBS and filtered using a Falcon® 40µm Cell Strainer (Corning, Cat#352340) and pelleted at 300g for 5 min. Cells were lysed with ACK lysing buffer (LifeTech, A10492-01), centrifuged at 300g for 5 min, resuspended at RT in PBS without Ca^{2+} or Mg^{2+} (LifeTech, Cat# 14190-136). Cells were pelleted, and total RNA was extracted from the pellet using a RNeasy Mini Kit (Qiagen, Cat No./ID: 74106). Reverse transcription was performed using a Reverse Transcriptase SuperScript® IV kit (ThermoFisher Cat #18090010) with random hexamer primers (ThermoFisher, Cat# 48190-011) according to manufacturer's instructions. The cDNA was then used as template for a first round PCR using Phusion Hot Start Flex DNA Polymerase (NEB, Cat# M0535; and the parameters were: initial denaturation 98°C 30s, then 25 cycles of 98°C, 10s; 60°C, 30s; 72°C, 60s; final extension 72°C 10 min; hold 4°C. PCR product was purified using Ampure XP beads (Beckman Coulter Cat# A63880), and used as template for a second round of PCR using the same kit as before with the parameters: initial denaturation 98°C, 30s; then 15 cycles of 98°C, 10s; 60°C, 30s; 72°C, 30s; final extension 72°C 10 min; hold 4°C. PCR amplicons were purified using a gel purification kit (ThermoFisher PureLink). DNA for each sample was quantified by qPCR (Kapa Biosystems) using qPCR machine. Sample DNA was used to make the 10 nM library and the library adjusted to 4 nM with pure distilled H_2O. The library was denatured using Phi X and NaOH according to the manufacturer's instructions (MiSeq Reagent Kit v3, 600 cycles), and mixed (70%) with Phi X (30%) and loaded onto an Illumina MiSeq and run overnight.

The Cigunpaired pipeline was developed to automate and scale up the following processes. First, the pRESTO suite of utilities (https://presto.readthedocs.io/en/stable/) was used to merge paired-end amplicon reads, filter out low-quality reads, mask primers, and deduplicate sequences. Unique sequences were annotated using Igblast (https://ncbi.github.io/igblast/) against a database containing mouse germline V, D, and J genes and the CH103.UCA KI genes. Non-functional reads with early stop codons or frame shifts were removed.

B cell lineage phylogenetic trees. Ig repertoire NGS fasta files were annotated using IgBlast and then cleaned to remove sequences containing stop codons, retaining only V_H sequences of the same length as UCA CH103. The cleaned sequences were aligned using Clustalx. A phylogenetic tree was built using IQ-TREE. Every non-leaf node in the tree is traversed. Nodes were collapsed if more than 70% of leaves in one node shared a common isotype, *i.e.*, IgA, IgM, IgG1, IgG2b, or IgG3.

Antibody variable region logoplots. Logoplots showing the frequency of SHM in elicited CH103 antibody heavy chains (V_H) were generated from bulk Ig transcript repertoire NGS data for mouse 201, 211, 224, 225, 226, 231, 232, 233, 239, 240, and 241. NGS transcripts were first annotated using IgBLAST. Only transcripts equal to the full-length UCA CH103 were retained, and the UCA sequence was removed prior to analysis. After alignment, the amino acid side chain occurrence at each position was counted. The resulting occurrence table was used as input for the Logomaker software (https://logomaker.readthedocs.io/en/latest/) to generate the logoplots.

Analysis of antibody SHM probability. Heavy and light chain sequences from Ig repertoire NGS were chosen manually from MEL immunized mice (study MEL01) and aligned with CH103.UCA and CH103.mat sequences. The probability of SHM occurrence was calculated using the program ARMADiLLO (https://armadillo.dhvi.duke.edu/)[44]. All SHM's probabilities were extracted from the ARMADiLLO outputs and merged into one representation shown by highlighting residues in different colors, as indicated.

Negative-stain EM of Fab–Env complexes. Fab (CH103.mat or H17L8) was incubated with CH505.TF or CH505.N197D mEnv at an approximately fivefold molar excess of Fab to trimer for 3 h. Complexes were diluted to ~0.03 mg ml^{-1} in Tris-buffered saline (50 mM Tris, pH 7.4, 150 mM NaCl), adsorbed onto glow-discharged copper mesh grids, and stained with 2% (w/v) uranyl formate for 60 s. Automated data collection was performed using EPU on a Thermo Scientific Talos F200C TEM equipped with a Ceta 16M camera, operated at 200 kV with a 2.0 Å pixel size and 73,000× magnification. Particle picking, 2D classification, ab initio reconstruction and 3D refinement were performed in cryoSPARC[68].

Cryo-EM. CH103 H17:L8 IgG was engineered with an HRV3C protease cleavage site (sequence: LEVLFQGP) in the heavy chain hinge region. The Fab fragment was generated by digesting 1 mg of IgG with 10 units of HRV3C protease (Pierce) incubating overnight at 4°C. HRV3C enzyme and Fc fragments were depleted by addition of 1/5th reaction volume of Protein A Sepharose (ThermoFisher) and Ni-NTA agarose (Qiagen), respectively, and incubating for 1 hour at RT. JRFL.TD15 mEnv was produced and purified as detailed above. BG505/CH505wk4 SOSIP containing additional A281V.Q293K.N295E mutations, is described in Pratap PP, *et al*[69].

Next, 150 µg purified JRFL.TD15 was mixed with a 60-fold molar excess of peptidisc (~187.5 µg) and gently rocked at 4°C in a 1.5 ml microcentrifuge tube. After 1 hour, 50 mg of activated Bio-beads were added to the solution and 1X Tris-buffered saline was added until the volume in the tube was ~1 ml. After an overnight incubation rocking at 4°C, the solution was separated from the Bio-beads through aspiration with a pipette. The solution was placed in a 100 kDa Molecular weight concentrator (Merck Amicon UFC5100) and centrifuged at 12,000xg until the sample volume was ~50 µl. The sample was then transferred to a new 1.5 ml microcentrifuge tube and H17:L8 Fab was added at a 3-fold molar excess (~105 µg). This mixture was incubated overnight at 4°C and then injected over a Superdex 200 Increase 10/300 GL (Cytiva #28990944) SEC column to purify the JRFL.TD15- H17:L8-Peptidisc complex. For mature CH103, 0.3 mg each of CH103 and RM19R Fab (added to increase angular sampling) were incubated with 0.2 mg BG505/CH505wk4 SOSIP overnight at 22°C and purified over a Superdex 200 Increase 10/300 GL (Cytiva #28990944) SEC column. Purified samples were concentrated to ~5-6 mg/ml and applied to holey carbon Quantifoil 1.2/1.3 300 mesh copper grids. The grids were plunge frozen using a Vitrobot Mark IV (ThermoFisher) at 4°C, 100% humidity, a blot force of 2, a 10 sec wait, and a 5 sec blot time. The grids were imaged using a 300 keV Titan Krios TEM (ThermoFisher) with a Gatan K2 Summit direct electron detector (BG505/CH505 + CH103) or a Gatan K3 direct electron detector and GIF BioQuantum energy filter (JRFL + CH103.H17L8). For the H17:L8 complex, data were collected at 105,000x magnification, a pixel size of 0.833 Å, an approximate total dose of 40.4 $e^-/Å^2$, and a defocus range of -0.8 µm to -1.5 µm. A total of 4,751 movie micrographs were collected for further processing. For the mature CH103 complex, data were collected at 29,000x magnification, a pixel size of 1.026 Å, an approximate total dose of 51.5 $e^-/Å^2$, and a defocus range of -0.8 µm to -1.8 µm. Both collections were performed using the Leginon[70] software package.

Initial preprocessing was done using the Appion package[71]. Frame alignment and dose weighting were performed using MotionCor2[72]. All further processing was done using cryoSPARC[68] (H17:L8 complex) or RELION 3.1[73] (mature CH103 complex). For H17:L8 complex processing in cryoSPARC, CTF estimation was calculated using Patch CTF. The micrographs were then curated based off CTF resolution estimate fits, with all micrographs outside the range of 2.478 Å – 5 Å being excluded. Particles were picked from the remaining micrographs using a blob picker. After a round of 2D classification, clean 2D classes were used to re-pick particles using a template picker. Further rounds of 2D classification were done to remove junk particles from the stack. The clean stack of particles was then used to generate a

reference volume using *ab initio* reconstruction. This reference volume was then refined using NU-refinement with a C1 symmetry and 3.2 Å resolution. The resulting refined volume was then used as the map for model building. For RELION data processing of the mature CH103 complex, CTF estimations were performed using Gctf, particle picks were imported from Appion, and standard 2D and 3D pipelines were followed. The final refined particle stack was also subjected to particle polishing before a final, C3 symmetry refinement resulting in a 2.8 Å reconstruction. A summary of all data collection and processing statistics can be found in Supplemental Table 7.

The initial structures for model building were generated from their amino acid sequence using ColabFold[74]. The initial models were then fit into the map using ChimeraX[75]. Manual adjustment was done using Coot[76] and further refinement was done using PHENIX[77] and Rosetta Relax[78]. Final model statistics are summarized in Supplemental Table 7. Buried surface areas (BSAs) were calculated using PDBePISA[79], with antibody contacts defined as residues contributing ≥15 Å² BSA. Maps and models were deposited in the EMDB and PDB, respectively, under the accession codes listed in Supplementary Table 7.

References

1. Nkolola, J.P. & Barouch, D.H. Prophylactic HIV-1 vaccine trials: past, present, and future. *The lancet. HIV* **11**, e117–e124 (2024).

2. Haynes, B.F. *et al.* Strategies for HIV-1 vaccines that induce broadly neutralizing antibodies. *Nat Rev Immunol* **23**, 142–158 (2023).

3. Burton, D.R. Advancing an HIV vaccine; advancing vaccinology. *Nat Rev Immunol* **19**, 77–78 (2019).

4. Overbaugh, J. & Morris, L. The Antibody Response against HIV-1. *Cold Spring Harb Perspect Med* **2**, a007039 (2012).

5. Wu, X. *et al.* Rational design of envelope identifies broadly neutralizing human monoclonal antibodies to HIV-1. *Science* **329**, 856–861 (2010).

6. Dam, K.A. *et al.* Mapping essential somatic hypermutations in a CD4-binding site bNAb informs HIV-1 vaccine design. *Cell Rep* **44**, 115713 (2025).

7. Gao, F. *et al.* Cooperation of B cell lineages in induction of HIV-1-broadly neutralizing antibodies. *Cell* **158**, 481–491 (2014).

8. Scheid, J.F. *et al.* Sequence and structural convergence of broad and potent HIV antibodies that mimic CD4 binding. *Science* **333**, 1633–1637 (2011).

9. Schommers, P. *et al.* Restriction of HIV-1 Escape by a Highly Broad and Potent Neutralizing Antibody. *Cell* **180**, 471–489.e422 (2020).

10. Liao, H.X. *et al.* Co-evolution of a broadly neutralizing HIV-1 antibody and founder virus. *Nature* **496**, 469–476 (2013).

11. Zhou, T. *et al.* Structural Repertoire of HIV-1-Neutralizing Antibodies Targeting the CD4 Supersite in 14 Donors. *Cell* **161**, 1280–1292 (2015).

12. Corti, D. *et al.* Analysis of memory B cell responses and isolation of novel monoclonal antibodies with neutralizing breadth from HIV-1-infected individuals. *PLoS One* **5**, e8805 (2010).

13. Chen, X. *et al.* Vaccination induces maturation in a mouse model of diverse unmutated VRC01-class precursors to HIV-neutralizing antibodies with >50% breadth. *Immunity* **54**, 324–339.e328 (2021).

14. Huang, D. *et al.* B cells expressing authentic naive human VRC01-class BCRs can be recruited to germinal centers and affinity mature in multiple independent mouse models. *Proc Natl Acad Sci U S A* **117**, 22920–22931 (2020).

15. Leggat, D.J. *et al.* Vaccination induces HIV broadly neutralizing antibody precursors in humans. *Science* **378**, eadd6502 (2022).

16. Jardine, J.G. *et al.* HIV-1 broadly neutralizing antibody precursor B cells revealed by germline-targeting immunogen. *Science* **351**, 1458–1463 (2016).

17. Saunders, K.O. *et al.* Targeted selection of HIV-specific antibody mutations by engineering B cell maturation. *Science* **366** (2019).

18. Lin, Y.R. *et al.* HIV-1 VRC01 Germline-Targeting Immunogens Select Distinct Epitope-Specific B Cell Receptors. *Immunity* **53**, 840–851.e846 (2020).

19. Saunders, K.O. *et al.* Vaccine induction of CD4-mimicking HIV-1 broadly neutralizing antibody precursors in macaques. *Cell* **187**, 79–94.e24 (2024).

20. Caniels, T.G. *et al.* Germline-targeting HIV-1 Env vaccination induces VRC01-class antibodies with rare insertions. *Cell reports. Medicine* **4**, 101003 (2023).

21. Gristick, H.B. *et al.* CD4 binding site immunogens elicit heterologous anti-HIV-1 neutralizing antibodies in transgenic and wild-type animals. *Sci Immunol* **8**, eade6364 (2023).

22. Williams, W.B. *et al.* Initiation of HIV neutralizing B cell lineages with sequential envelope immunizations. *Nat Commun* **8**, 1732 (2017).

23. Verkoczy, L. *et al.* Induction of HIV-1 broad neutralizing antibodies in 2F5 knock-in mice: selection against membrane proximal external region-associated autoreactivity limits T-dependent responses. *J Immunol* **191**, 2538–2550 (2013).

24. McGuire, A.T. *et al.* Specifically modified Env immunogens activate B-cell precursors of broadly neutralizing HIV-1 antibodies in transgenic mice. *Nat Commun* **7**, 10618 (2016).

25. Leaman, D.P., Stano, A., Chen, Y., Zhang, L. & Zwick, M.B. Membrane Env Liposomes Facilitate Immunization with Multivalent Full-Length HIV Spikes. *J Virol* **95**, e0000521 (2021).

26. Guenaga, J. *et al.* Vaccination generates broadly cross-neutralizing antibodies to the HIV Env apex. *Nature* (2026).

27. Zhang, J. *et al.* Binding dynamics shape germinal center broadly neutralizing responses to HIV priming. *bioRxiv* (2026).

28. Sanders, R.W. *et al.* Stabilization of the soluble, cleaved, trimeric form of the envelope glycoprotein complex of human immunodeficiency virus type 1. *J Virol* **76**, 8875–8889 (2002).

29. Del Moral-Sánchez, I. *et al.* High thermostability improves neutralizing antibody responses induced by native-like HIV-1 envelope trimers. *NPJ vaccines* **7**, 27 (2022).

30. Kong, L. *et al.* Uncleaved prefusion-optimized gp140 trimers derived from analysis of HIV-1 envelope metastability. *Nat Commun* **7**, 12040 (2016).

31. Crispin, M., Ward, A.B. & Wilson, I.A. Structure and Immune Recognition of the HIV Glycan Shield. *Annual review of biophysics* (2018).

32. Torrents de la Pena, A. *et al.* Similarities and differences between native HIV-1 envelope glycoprotein trimers and stabilized soluble trimer mimetics. *PLoS Pathog* **15**, e1007920 (2019).

33. Cao, L. *et al.* Differential processing of HIV envelope glycans on the virus and soluble recombinant trimer. *Nat Commun* **9**, 3693 (2018).

34. Lee, J.H., Ozorowski, G. & Ward, A.B. Cryo-EM structure of a native, fully glycosylated, cleaved HIV-1 envelope trimer. *Science* **351**, 1043–1048 (2016).

35. Guenaga, J. *et al.* Structure-Guided Redesign Increases the Propensity of HIV Env To Generate Highly Stable Soluble Trimers. *J Virol* **90**, 2806–2817 (2015).

36. Leaman, D.P. & Zwick, M.B. Increased functional stability and homogeneity of viral envelope spikes through directed evolution. *PLoS Pathog* **9**, e1003184 (2013).

37. Pearce, E.J., La Flamme, A., Sabin, E. & Brunet, L.R. The initiation and function of Th2 responses during infection with Schistosoma mansoni. *Advances in experimental medicine and biology* **452**, 67–73 (1998).

38. Nabors, G.S., Afonso, L.C., Farrell, J.P. & Scott, P. Switch from a type 2 to a type 1 T helper cell response and cure of established Leishmania major infection in mice is induced by combined therapy with interleukin 12 and Pentostam. *Proc Natl Acad Sci U S A* **92**, 3142–3146 (1995).

39. Peterson, K.E., Stromnes, I., Messer, R., Hasenkrug, K. & Chesebro, B. Novel role of CD8(+) T cells and major histocompatibility complex class I genes in the generation of protective CD4(+) Th1 responses during retrovirus infection in mice. *J Virol* **76**, 7942–7948 (2002).

40. Tam, H.H. *et al.* Sustained antigen availability during germinal center initiation enhances antibody responses to vaccination. *Proc Natl Acad Sci U S A* **113**, E6639–E6648 (2016).

41. Silva, M. *et al.* A particulate saponin/TLR agonist vaccine adjuvant alters lymph flow and modulates adaptive immunity. *Sci Immunol* **6**, eabf1152 (2021).

42. Cheng, H.D. *et al.* Fine epitope signature of antibody neutralization breadth at the HIV-1 envelope CD4-binding site. *JCI insight* **3** (2018).

43. Setliff, I. *et al.* High-Throughput Mapping of B Cell Receptor Sequences to Antigen Specificity. *Cell* **179**, 1636–1646.e1615 (2019).

44. Martin Beem, J.S., Venkatayogi, S., Haynes, B.F. & Wiehe, K. ARMADiLLO: a web server for analyzing antibody mutation probabilities. *Nucleic Acids Res* **51**, W51–w56 (2023).

45. Liu, Q. *et al.* Acquisition of quaternary trimer interaction as a key step in the lineage maturation of a broad and potent HIV-1 neutralizing antibody. *Structure* (2025).

46. Fera, D. *et al.* Affinity maturation in an HIV broadly neutralizing B-cell lineage through reorientation of variable domains. *Proc Natl Acad Sci U S A* **111**, 10275–10280 (2014).

47. Adolf-Bryfogle, J. *et al.* RosettaAntibodyDesign (RAbD): A general framework for computational antibody design. *PLoS computational biology* **14**, e1006112 (2018).

48. Zhou, J.O., Zaidi, H.A., Ton, T. & Fera, D. The Effects of Framework Mutations at the Variable Domain Interface on Antibody Affinity Maturation in an HIV-1 Broadly Neutralizing Antibody Lineage. *Front Immunol* **11**, 1529 (2020).

49. Abramson, J. *et al.* Accurate structure prediction of biomolecular interactions with AlphaFold 3. *Nature* **630**, 493–500 (2024).

50. LaBranche, C.C. *et al.* Neutralization-guided design of HIV-1 envelope trimers with high affinity for the unmutated common ancestor of CH235 lineage CD4bs broadly neutralizing antibodies. *PLoS Pathog* **15**, e1008026 (2019).

51. Bonsignori, M. *et al.* Two Distinct Broadly Neutralizing Antibody Specificities of Different Clonal Lineages in a Single HIV-1-infected Donor: Implications for Vaccine Design. *J Virol* (2012).

52. Bonsignori, M. *et al.* Maturation Pathway from Germline to Broad HIV-1 Neutralizer of a CD4-Mimic Antibody. *Cell* **165**, 449–463 (2016).

53. Zhou, T. *et al.* Structural basis for broad and potent neutralization of HIV-1 by antibody VRC01. *Science* **329**, 811–817 (2010).

54. Schleich, F.A. *et al.* Vaccination of nonhuman primates elicits a broadly neutralizing antibody lineage targeting a quaternary epitope on the HIV-1 Env trimer. *Immunity* **58**, 1598–1613.e1598 (2025).

55. Ramezani-Rad, P. *et al.* The saponin monophosphoryl lipid A nanoparticle adjuvant induces dose-dependent HIV vaccine responses in non-human primates. *J Clin Invest* (2025).

56. Lee, J.H. *et al.* Long-primed germinal centres with enduring affinity maturation and clonal migration. *Nature* **609**, 998–1004 (2022).

57. Lenart, K. *et al.* Three immunizations with Novavax's protein vaccines increase antibody breadth and provide durable protection from SARS-CoV-2. *NPJ vaccines* **9**, 17 (2024).

58. Yeh, C.H. *et al.* Induction of multiple HIV-1 neutralizing B Cell Precursors in Humans. *medRxiv : the preprint server for health sciences* (2026).

59. Morris, D.J. *et al.* Transient glycan shield reduction induces CD4-binding site broadly neutralizing antibodies in SHIV-infected macaques. *Cell Rep* **44**, 115848 (2025).

60. Saunders, K.O. *et al.* Stabilized HIV-1 envelope immunization induces neutralizing antibodies to the CD4bs and protects macaques against mucosal infection. *Sci Transl Med* **14**, eabo5598 (2022).

61. Agrawal, N. *et al.* Functional Stability of Unliganded Envelope Glycoprotein Spikes among Isolates of Human Immunodeficiency Virus Type 1 (HIV-1). *PLoS One* **6**, e21339 (2011).

62. Mangala Prasad, V. *et al.* Cryo-ET of Env on intact HIV virions reveals structural variation and positioning on the Gag lattice. *Cell* **185**, 641–653.e617 (2022).

63. Wei, X. *et al.* Emergence of resistant human immunodeficiency virus type 1 in patients receiving fusion inhibitor (T-20) monotherapy. *Antimicrob Agents Chemother* **46**, 1896–1905 (2002).

64. Montefiori, D.C. Measuring HIV neutralization in a luciferase reporter gene assay. *Methods Mol Biol* **485**, 395–405 (2009).

65. Stano, A. *et al.* Dense array of spikes on HIV-1 virion particles. *J Virol* **91**, 415–417 (2017).

66. Saunders, K.O. *et al.* Vaccine Induction of Heterologous Tier 2 HIV-1 Neutralizing Antibodies in Animal Models. *Cell Rep* **21**, 3681–3690 (2017).

67. Ota, T. *et al.* Anti-HIV B Cell lines as candidate vaccine biosensors. *J Immunol* **189**, 4816–4824 (2012).

68. Punjani, A., Rubinstein, J.L., Fleet, D.J. & Brubaker, M.A. cryoSPARC: algorithms for rapid unsupervised cryo-EM structure determination. *Nat Methods* **14**, 290–296 (2017).

69. Pratap, P.P. *et al.* Immunofocusing on the conserved fusion peptide of HIV envelope glycoprotein in rhesus macaques. *bioRxiv* (2024).

70. Suloway, C. *et al.* Automated molecular microscopy: the new Leginon system. *J Struct Biol* **151**, 41–60 (2005).

71. Lander, G.C. *et al.* Appion: an integrated, database-driven pipeline to facilitate EM image processing. *J Struct Biol* **166**, 95–102 (2009).

72. Zheng, S.Q. *et al.* MotionCor2: anisotropic correction of beam-induced motion for improved cryo-electron microscopy. *Nat Methods* **14**, 331–332 (2017).

73. Zivanov, J., Nakane, T. & Scheres, S.H.W. Estimation of high-order aberrations and anisotropic magnification from cryo-EM data sets in RELION-3.1. *IUCrJ* **7**, 253–267 (2020).

74. Mirdita, M. *et al.* ColabFold: making protein folding accessible to all. *Nat Methods* **19**, 679–682 (2022).

75. Goddard, T.D. *et al.* UCSF ChimeraX: Meeting modern challenges in visualization and analysis. *Protein Sci* **27**, 14–25 (2018).

76. Emsley, P. & Cowtan, K. Coot: model-building tools for molecular graphics. *Acta crystallographica. Section D, Biological crystallography* **60**, 2126–2132 (2004).

77. Afonine, P.V. *et al.* Real-space refinement in PHENIX for cryo-EM and crystallography. *Acta crystallographica. Section D, Structural biology* **74**, 531–544 (2018).

78. Conway, P., Tyka, M.D., DiMaio, F., Konerding, D.E. & Baker, D. Relaxation of backbone bond geometry improves protein energy landscape modeling. *Protein Sci* **23**, 47–55 (2014).

79. Krissinel, E. & Henrick, K. Inference of macromolecular assemblies from crystalline state. *J Mol Biol* **372**, 774–797 (2007).

80. Jia, M. *et al.* VSV-Displayed HIV-1 Envelope Identifies Broadly Neutralizing Antibodies Class-Switched to IgG and IgA. *Cell Host Microbe* **27**, 963–975.e965 (2020).

MAIN FIGURES

Figure 1.

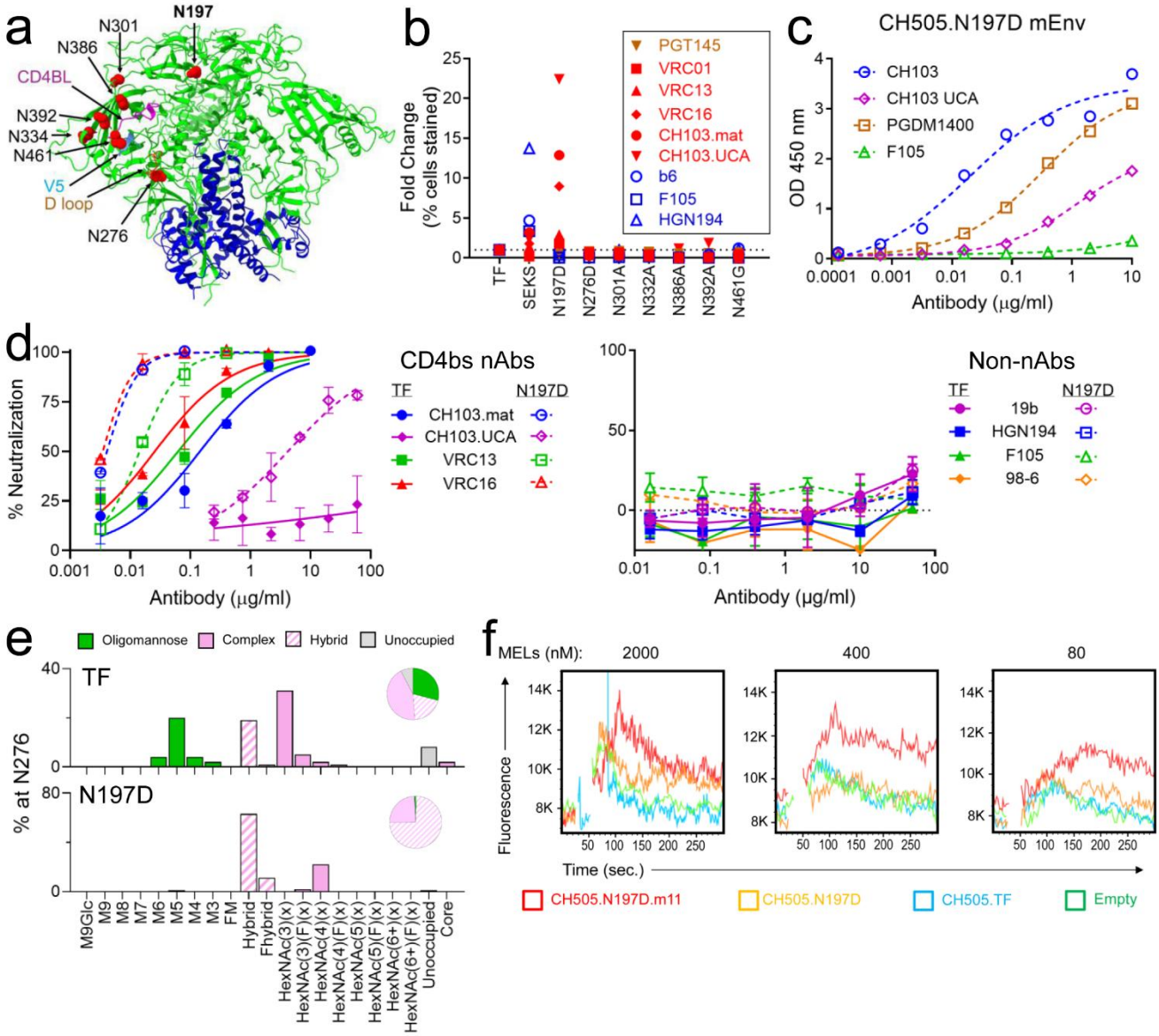


Fig. 1 | N197D selectively enhances CH103.UCA recognition and B-cell activation by CH505 membrane Env.

a, Model of trimeric Env (PDB: 6VY2[80]) showing N197 and other NLG near the CD4bs that were mutated for analysis by flow cytometry.

b, Flow-cytometric staining of HEK293T cells expressing the indicated CH505 NLG mutants or cleavage-deficient SEKS Env with CD4bs bnAbs and non-nAbs. Fold change in percentage of cells stained relative to CH505.TF-transduced cells was calculated from flow cytometry experiment performed in duplicate.

c, ELISA in which lectin-captured, crosslinked/purified CH505.N197D mEnv was probed with CH103.UCA, CH103.mat, PGDM1400 (V2 quaternary bnAb), and F105. Representative assay is shown.
d, CH505.N197D mutant virus is more sensitive than CH505.TF to several CD4bs bnAbs in a neutralization assay, is neutralized by CH103.UCA (left), but is not sensitive to several non-nAbs (right). Representative assay performed in duplicate is shown.
e, Glycosylation composition analysis of CH505.TF and CH505.N197D mEnvs at the N276 NLG site. Detailed categories are shown for oligomannose (green), hybrid-type (pink striped), and complex-type (pink) glycans, as well as the proportion of unoccupied NLG (grey).
f, Activation of *ex vivo* CH103.UCA B cells by CH505 MEL antigens measured over time. CH505.TF, CH505.N197D and CH505.N197D.m11 MELs were compared with empty liposomes at three mEnv trimer concentrations, or equivalent liposome amounts for empty liposomes. Data are from one experiment, with each antigen tested at three concentrations. Data are shown as mean fluorescence intensity (MFI).

Figure 2.

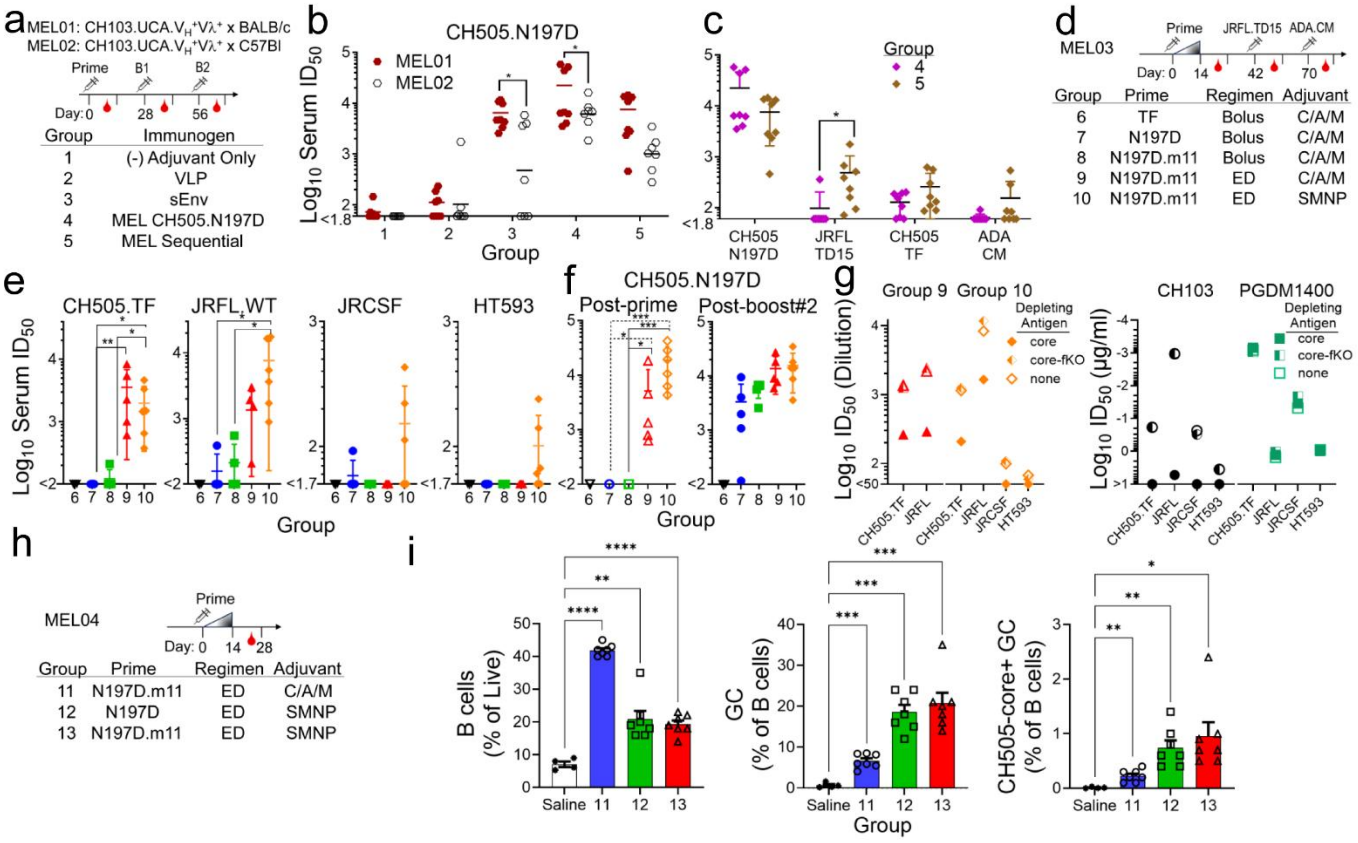


Fig. 2 | Sequential MEL immunization drives CH103-class GC responses and tier-2 HIV serum cross-neutralization.

a, MEL01 (CH103.UCA x Balb/c F1 cross) and MEL02 (CH103.UCA x C57Bl F1 cross) immunization regimen to test MEL activation in CH103.UCA het dKI mice. Mice received autologous CH505.N197D immunizations in different modalities vs MEL sequential immunization (group 5), which was primed with MEL CH505.N197D and boosted with MELs JRFL.TD15 (B1) and ADA.CM (B2). The same immunization was performed in mouse model haplotypes from crosses to BALB/c (MEL01) or C57Bl (MEL02). Group 1 was n=7, all other groups were n=8.

b, Sera from immunized mice (both MEL01 and MEL02) were harvested after boost 2 and were tested in a neutralization assay against CH505.N197D virus. The experiment was performed in triplicate. P values were calculated by Kruskal–Wallis test with Dunn's correction.

c, Serum neutralization of autologous and sequential immunogen-matched viruses in MEL01 group 4, which received CH505.N197D MELs only, and group 5, which received sequential MELs. The experiment was performed in triplicate. Groups were compared within each virus by two-tailed Mann–Whitney tests with Holm–Sidak correction for multiple comparisons.

d, MEL03 immunization regimen to test higher affinity GT immunogen, escalating dose (ED) priming, and SMNP adjuvant. Priming immunogens were administered by bolus or ED injections with C/A/M (CpG/Alum/MPLA) or SMNP adjuvant. Groups contained n=2 (Grp6), n=5 (Grps 7-9), and n=6 (Grp 10).

e, Serum neutralization after boost 2 against tier-2 viruses CH505.TF, JRFL, JRCSF, and HT593. Titers are plotted as $\log_{10}$ reciprocal serum dilution at 50% inhibition calculated from a representative experiment performed in triplicate. Each point represents one mouse; bars indicate median. Statistical analysis was performed as in **b**.

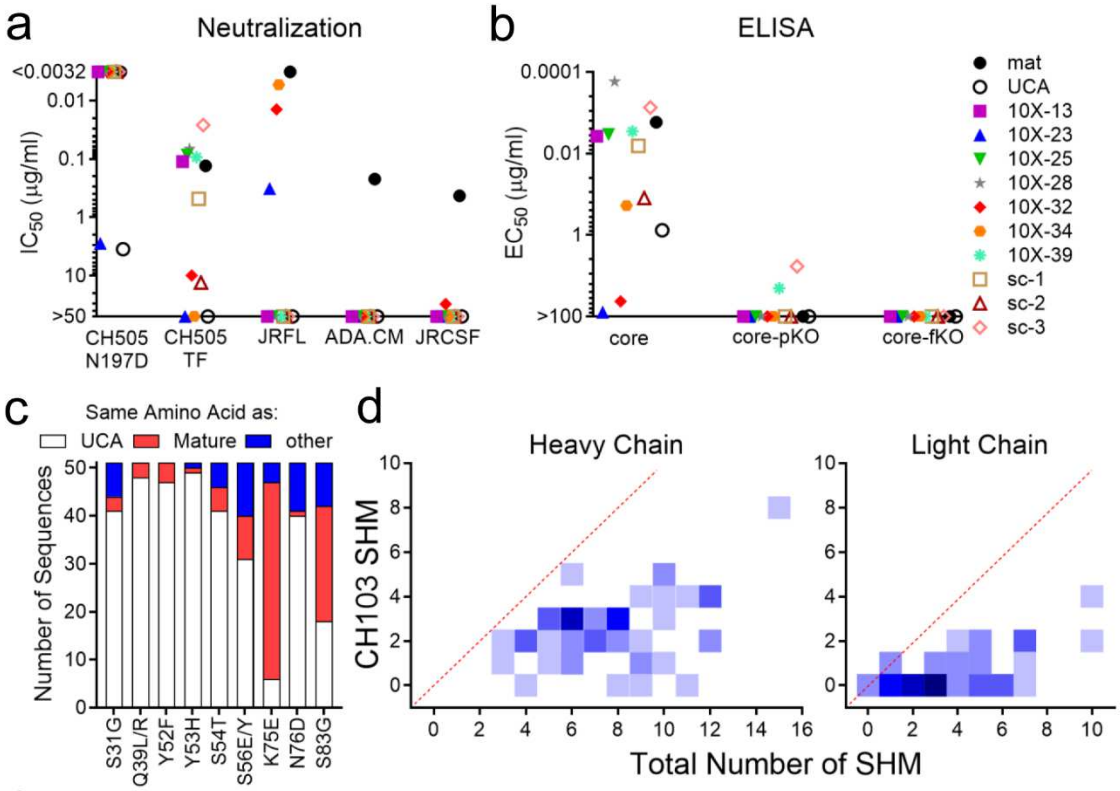
f, Serum neutralization of CH505.N197D virus after prime or boost 2. Statistical significance determination as in **b**.

g, Pooled sera from MEL03 Groups 9 and 10 (left panel), as well as control bnAbs CH103 and PGDM1400 (right panel), were depleted using CH505.gp120-core WT or fKO (D368R, E370A) that knocks out CD4bs antibody binding, or empty beads. Depleted samples were tested for neutralization activity. Open symbols indicate mock-depleted samples (empty beads), partially filled symbols indicate fKO core-depleted samples, and filled symbols indicate WT core-depleted samples.

h, Immunization schedule, immunogens and adjuvants used in study MEL04 in CH103.UCA heterozygous dKI mice, a study designed to test SMNP/ED-priming on early GC responses. All groups were n=6.

i, Flow-cytometric analysis of draining lymph node B cells harvested 10 days after priming and stained with CH505 gp120-core. Statistical significance was assessed by Brown–Forsythe and Welch ANOVA with Dunnett's T3 multiple-comparisons test, comparing each group with the saline control.

Figure 3.



e

	Total HC SHM	HCDR2	HFWR3	Total LC SHM	LCDR2	LFWR3	IC50 (µg/ml) JRFL	IC50 (µg/ml) CH505
CH103.UCA	0	51-IYYSGST-57	74-SKNQ-77	0	48-IYQDSK-53	65-SNS-67	>50	>50
CH103.mat	28	.FHT.E.	.ED.	24	.FENY.	.K.	0.005	0.13
10X-34	12	...T.Y.	.DD.	7	....N.	.K.	0.005	>50
10X-32	11	...T.Y.	.E.E	10	....Y.	.I.	0.014	9.9
10X-23	12	.....Y.	.E.E	10	....N.	.K.	0.32	>50
10X-28	7	.....	.E..	5	....F.	.S.	>50	0.067
10X-13	8	.....	.E..	5	.....	...	>50	0.11
10X-25	7	.....T.	.E..	3	.....	...	>50	0.085
10X-39	6	.....	.E..	3	....R.	...	>50	0.093
sc-1	5	...T...	.E..	2	.....	...	>50	0.48
sc-2	2	.....	.E..	1	.....	...	>50	13.1
sc-3	4	.....	.E..	3	....T.	...	>50	0.026

Fig. 3 | Single-cell antibody recovery reveals CH103-lineage neutralization after MEL immunization.

a, Antigen-specific B cells from MEL03 Groups 9 and 10 were single-cell sorted using CH505 gp120-core and trimeric Env probes and paired heavy- and light-chain sequences were recovered. Selected antibodies were expressed and tested for neutralization against CH505.N197D, CH505.TF, JRFL, ADA.CM and JRCSF viruses. IC_{50} values calculated from an assay performed in triplicate are shown.

b, Binding of antibodies from panel **a** to CH505.gp120-core as well as pKO and fKO CD4bs-knockout gp120-cores by ELISA. EC_{50} values calculated from an average of two independent assays performed singly are shown.

c, Stacked bar graph showing the relative abundance of amino-acid identities at selected CH103-lineage heavy-chain positions in sequenced antibodies. Residues are classified as germline-encoded, CH103.mat-identical, or other. Positions were selected for comparison with CH103.mat and for subsequent structure-guided and functional analysis.
d, Relationship between total SHM and mature CH103-identical SHM in heavy and light chains of 51 recombinant mAbs recovered by antigen-specific single-cell sorting from MEL03. Box shading indicates the number of sequences observed.
e, Sequence alignment of selected MEL03 single-cell antibodies showing SHM associated with JRFL neutralization. Mature CH103-identical SHM are highlighted in yellow.

Figure 4.

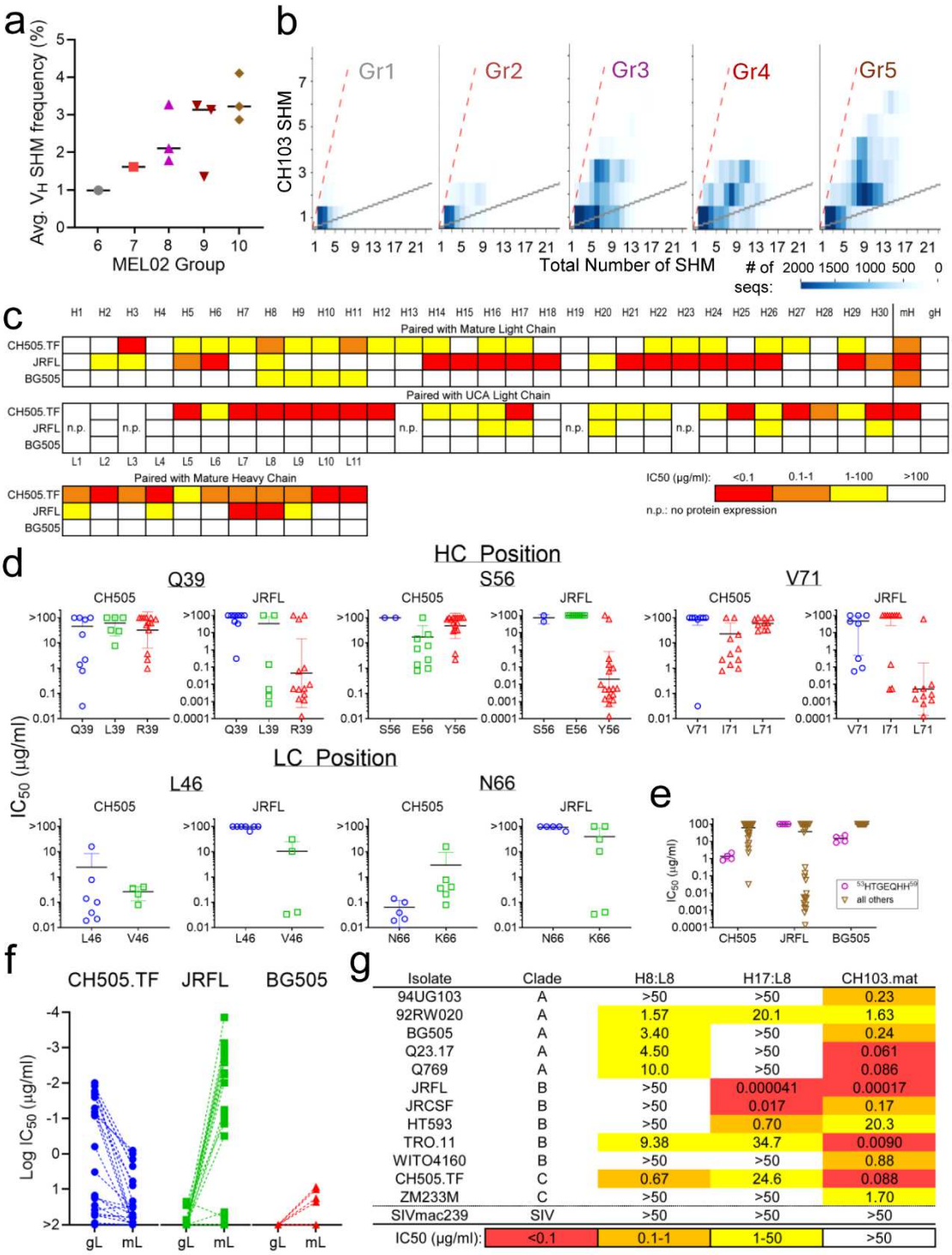


Fig. 4 | Repertoire-guided antibody pairing identifies CH103-class mutations linked to potent tier-2 cross-neutralization.

a, Median V_H mutation frequency in splenic B cells from selected MEL01 mice, determined by Ig repertoire sequencing.

b, Total heavy-chain amino-acid mutations and CH103.mat-identical substitutions in IgG1

sequences from each MEL01 mouse. The staggered gray line indicates the number of CH103.mat-identical substitutions expected by random chance, and the red dashed line marks the total number of CH103.mat-identical heavy-chain substitutions as a reference.

c, Neutralization activity of recombinant antibodies generated from 31 heavy chains and 14 light chains selected from MEL01 repertoire sequencing. Heavy chains were paired with either CH103.mat light chain (mL) or CH103.UCA light chain (gL), and selected light chains were paired with CH103.mat heavy chain (mH). Antibodies were tested in duplicate for neutralization of CH505.TF, JRFL and BG505. n.p., no protein production.

d, Association between amino-acid identity at selected CH103 positions and neutralization activity. IC_{50} values are shown for elicited heavy chains paired with mL or elicited light chains paired with mH. Blue circles denote CH103.UCA residues, green squares denote CH103.mat residues and red triangles denote novel SHM not present in either CH103.UCA or CH103.mat.

e, Alignment of four elicited heavy-chain sequences containing a 4–5-residue CDRH2 motif matching CH103.mat. Mature CH103-identical SHM are highlighted in grey and novel SHM in yellow.

f, Thirty-one heavy chains selected from repertoire sequencing were paired with either the CH103.UCA light chain or CH103.mat light chain. Reassortant antibodies were tested for neutralization of CH505.TF, JRFL and BG505, and the change in IC_{50} between germline and mature light-chain pairings is shown.

g, Two heavy chains with the greatest breadth and potency, H8 and H17, were paired with L8, the light chain that conferred the strongest activity when paired with CH103 mature heavy chain. The resulting reassortants, H8L8 and H17L8, were tested against a panel of CH103-sensitive HIV-1 isolates. IC_{50} values are calculated from the average of two experiments each performed in duplicate.

Figure 5.

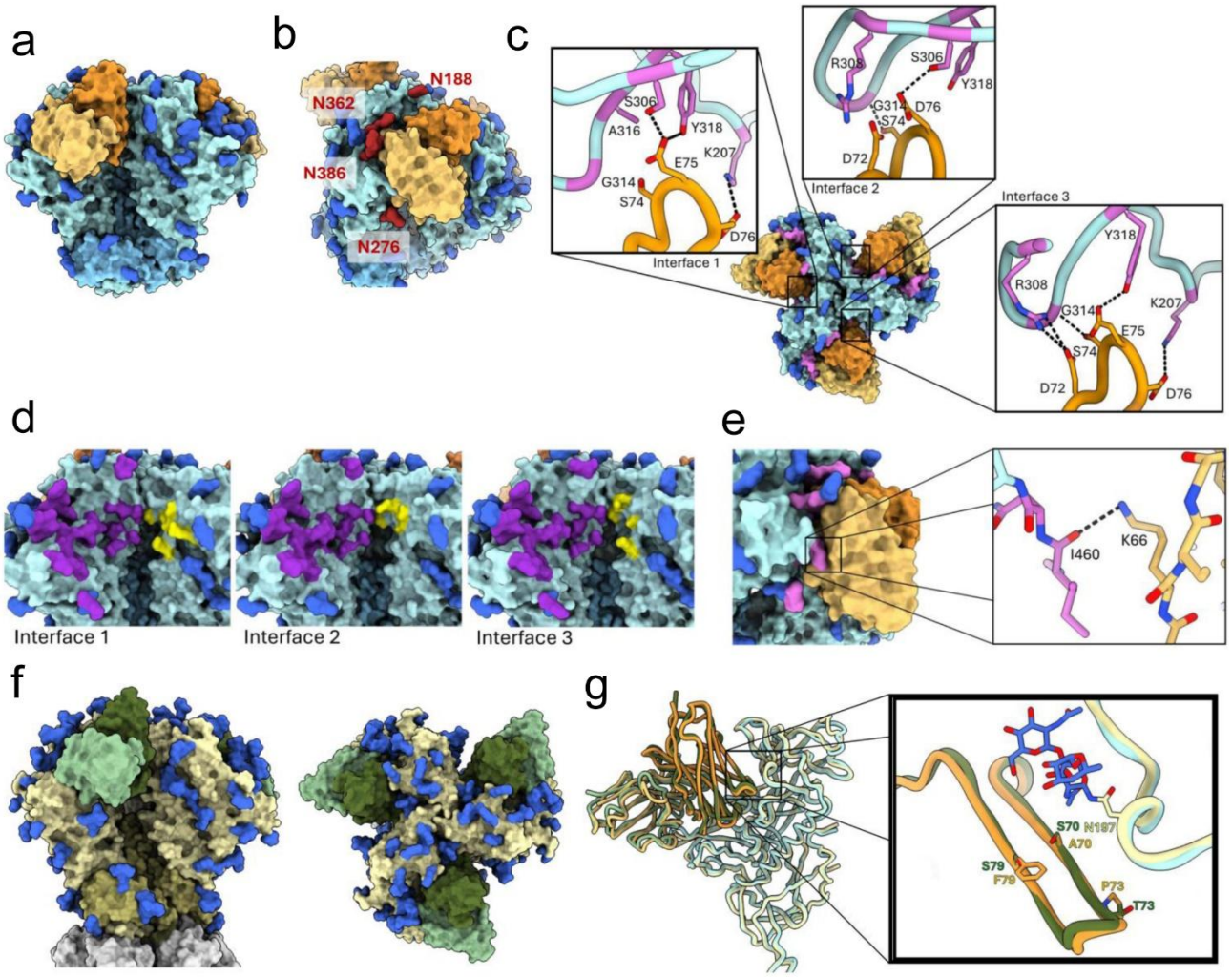


Fig. 5 | Cryo-EM reveals shared quaternary CD4bs recognition between infection and vaccine-derived CH103-lineage antibodies.

a, Cryo-EM structure of H17L8 bound to JRFL.TD15 Env, shown as a surface model. H17 heavy chain is orange, L8 light chain is yellow, gp120 is pale turquoise, gp41 is sky blue and modelled glycans are royal blue.

b, CD4bs-proximal glycans surrounding the H17L8 epitope on JRFL.TD15, with N188, N276, N362 and N386 highlighted in red.

c, Asymmetric engagement of JRFL.TD15 by H17L8. Quaternary contact residues are shown for each H17 heavy chain and its adjacent gp120 protomer.

d, JRFL.TD15 surface with H17L8 removed, showing epitope contact residues on the primary and adjacent gp120 protomers highlighted in purple and yellow, respectively. The three Fab–Env interfaces were analyzed independently.

e, Close-up of the hydrogen bond between L8 K66 and the gp120 V5 backbone at I460.
f, Cryo-EM structure of mature CH103 bound to CH505wk4.c Env, shown as a surface model. CH103 heavy and light chains are dark and light green, respectively; gp120 is pale yellow, gp41 is yellow and modelled glycans are royal blue.
g, Overlay of mature CH103 bound to CH505wk4.c gp120 and H17L8 bound to JRFL.TD15 gp120. The inset shows the position of the CH505wk4.c N197 glycan relative to the framework region 3 of mature CH103 and H17, with sequence differences indicated.

Figure 6.

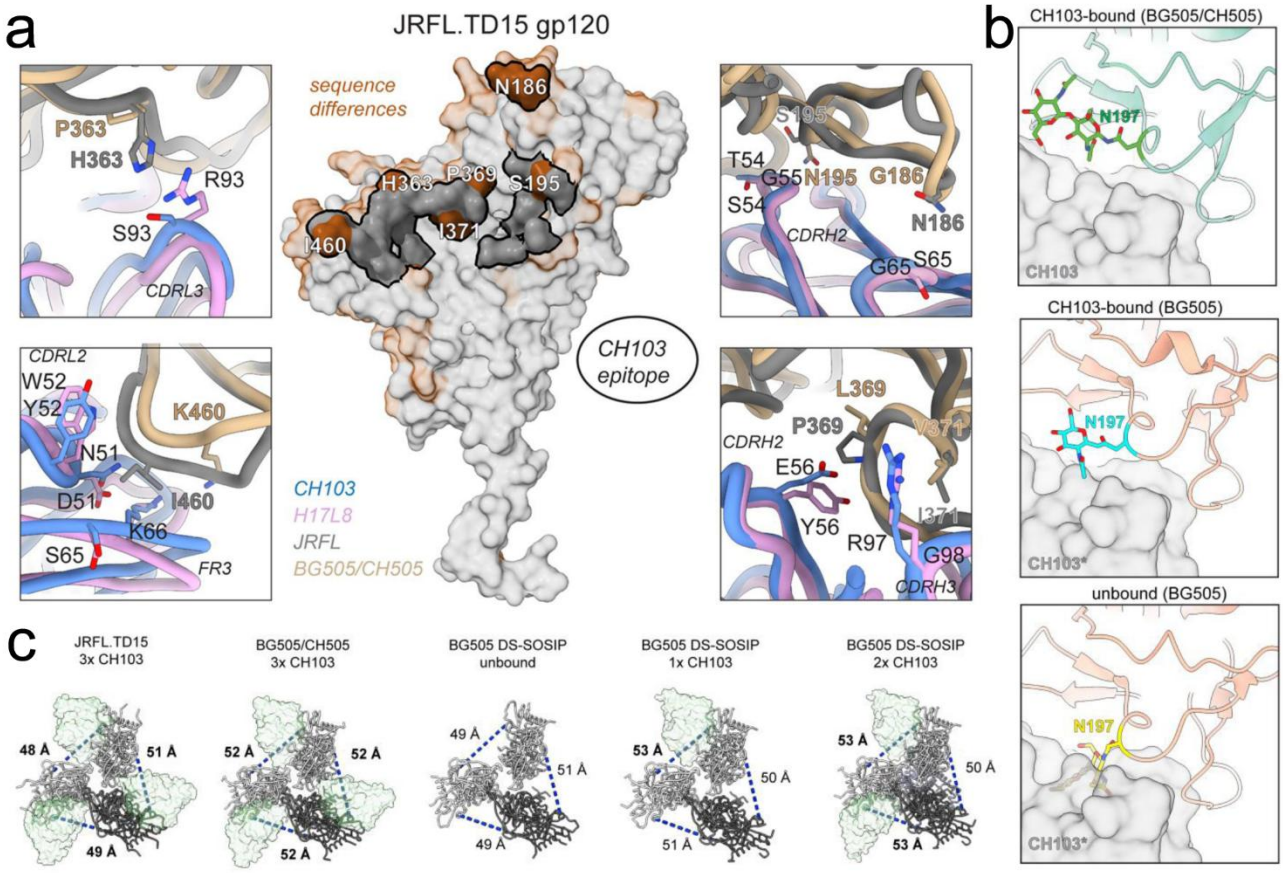


Fig. 6 | CH103-lineage antibodies converge on quaternary CD4bs recognition across distinct Env trimers.

a, Structural comparison of mature CH103 bound to CH505wk4.c and vaccine-derived H17L8 bound to JRFL.TD15 shows a shared quaternary CD4bs recognition mode across Env trimers with distinct local sequence and glycan features. JRFL.TD15 gp120 is shown as a surface, with regions that differ from CH505wk4.c colored brown. The CH103-class antibody footprint is outlined in black and shown in darker shading. Residues that differ between JRFL.TD15 and CH505wk4.c and lie within or near the antibody interface are labelled. Insets show local overlays of the JRFL.TD15–H17L8 and CH505wk4.c–CH103 complexes, with key residues shown as sticks.

b, Comparison of CH103-bound and unbound Env structures illustrates how N197 glycan positioning can be accommodated or displaced during CH103-lineage recognition. Middle, CH103-bound BG505 SOSIP trimer (PDB: 9D7P) showing similar displacement of the N197 glycan. Bottom, Unbound BG505 SOSIP trimer (PDB 9D7G), in which the N197 glycan is predicted to clash with CH103-class antibody binding. All structures used for N197 position comparison were aligned by gp120 to the CH103-bound BG505/CH505 structure**,** and the

relative position of CH103 from the reference structure is shown and designated with an asterisk.

c, Distances between gp120 interfaces as measured from the Cα atoms of N280 of one protomer to C445 of the adjacent protomer. Interfaces bound by CH103 are shown with transparent Fab Fv surfaces, with distance value in bold**.** Reference structures are as follows: PDB 9D7P (BG505 DS-SOSIP in complex with 2x CH103), PDB 9D7O (BG505 DS-SOSIP in complex with 1x CH103), and PDB 9D7G (unbound BG505 DS-SOSIP).

Figure 7.

a

ID	HC	LC	IC50 (μg/ml) CH505.N197D	CH505.TF	JRFL
UCA	none	none	1.54	>50	>50
min1	K75E	L46V	0.0059	14.5	>50
min2	K75E	none	0.049	>50	>50
min3	none	L46V	1.10	>50	>50
min5	Q39L.S56Y.K75E.N76D	D30S.K31T.Q50E.N66K	3.77	>50	5.52
min8	none	K27R.S52W.S93R	0.25	14.25	>50
min9	Q39L.S56Y.K75E.N76D	K27R.S52W.S93R	0.00039	0.0057	45.9
min11	S56Y.K75E	K27R.S52W.S93R	0.00047	0.31	12
min15	Y53H.S54T.S56Y.K75E.N76D.S83R	K27R.S52W.S93R	0.00032	0.013	1.61
	CH103 Homologs				
	HC	LC			
	IZ95W	CH103.UCA	>50	>50	>50
	IZ95W.K75E	CH103.UCA	0.0043	>50	>50
	021V4	CH103.UCA	>50	>50	>50
	021V4.K75E	CH103.UCA	0.038	>50	>50

IC_{50} (μg/ml) <0.1 | 0.1-1 | 1-50 | >50

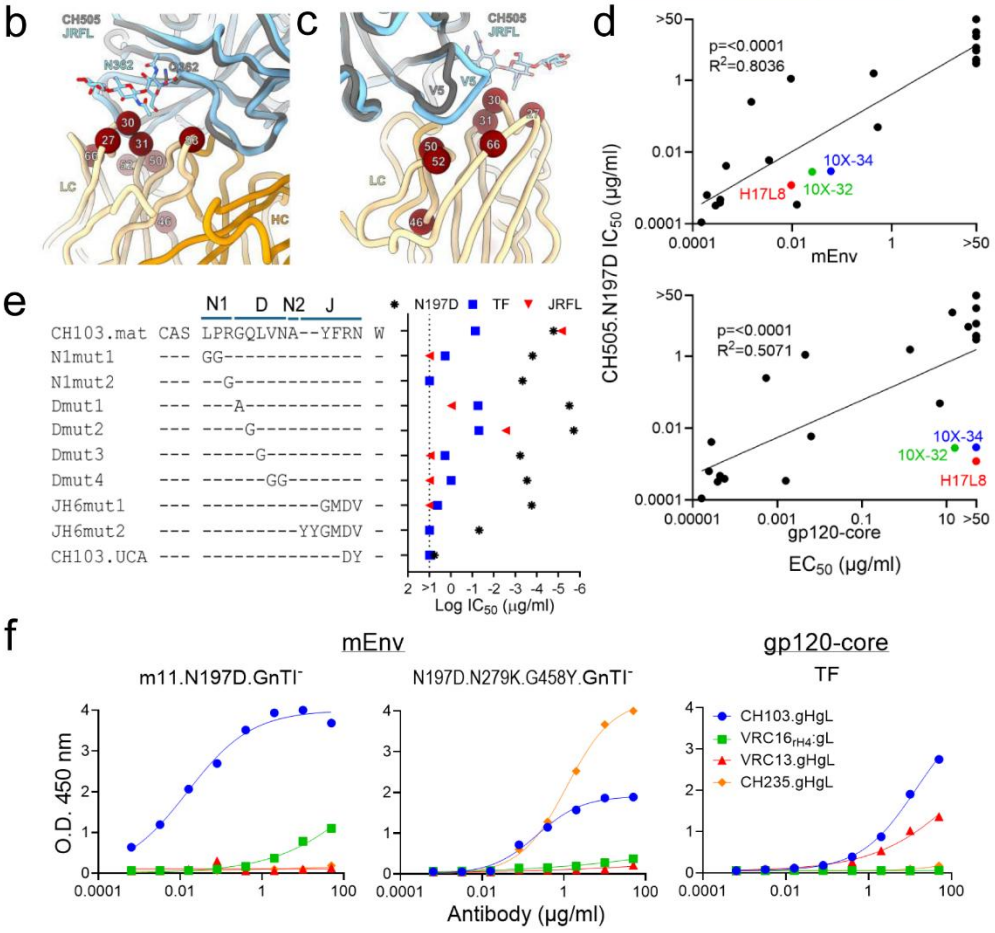


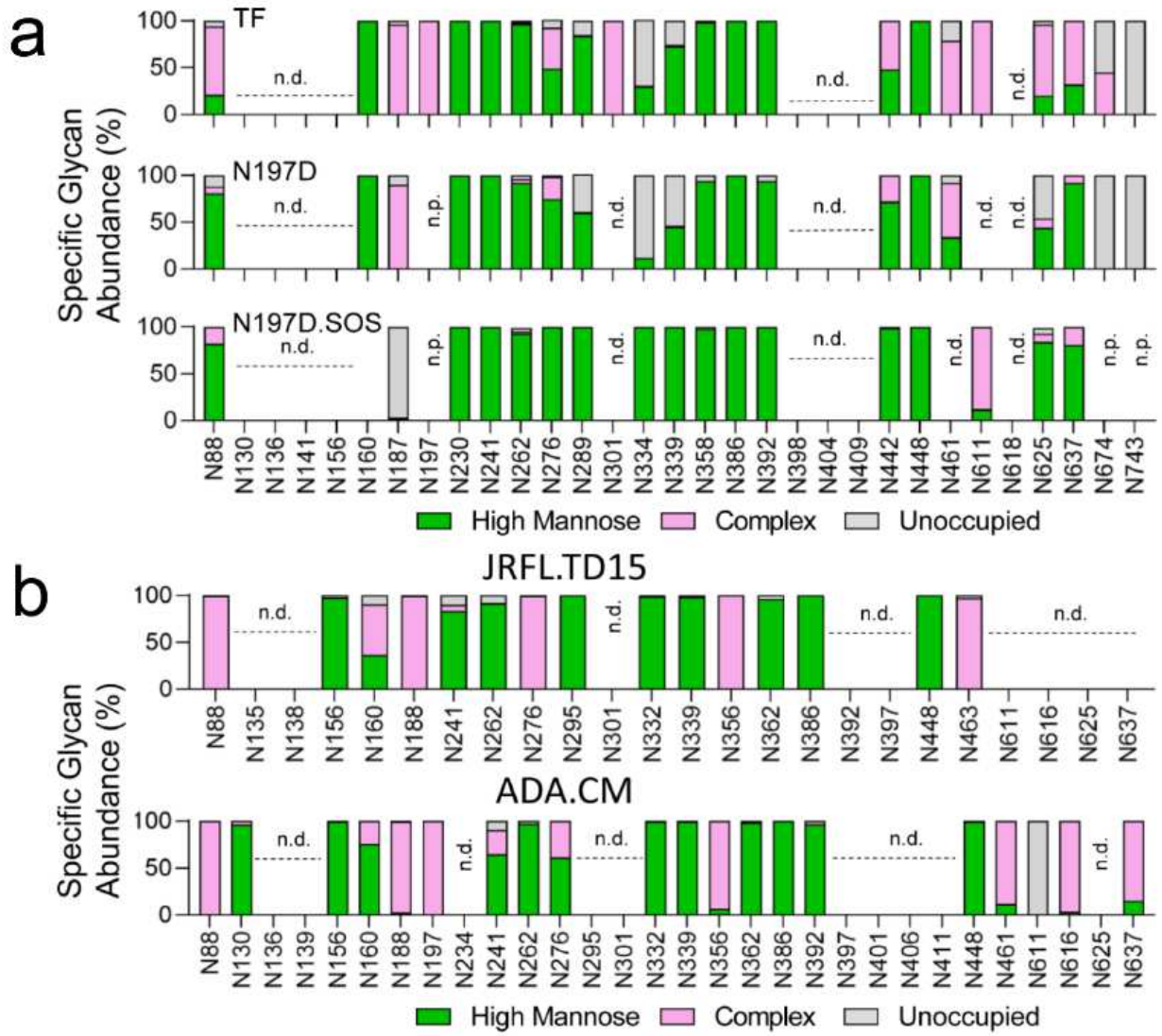
Fig. 7 | Minimal mutations and related Env variants reveal plasticity in germline targeting of H3-dominated class CD4bs precursors.

a, Neutralization activity of selected CH103.UCA-derived antibodies containing minimal somatic mutations against CH505.N197D, CH505.TF and JRFL viruses. IC_{50} values are calculated from the average of two experiments each performed in duplicate. The full panel of CH103.min antibodies is shown in **Extended Data Fig. 8b**.

b, AlphaFold3 models of selected CH103.min antibodies bound to JRFL or BG505/CH505 Env, aligned at the CD4bs and focused on the N362 glycan-proximal region. The close-up shows the predicted position of L-CDR1 relative to the JRFL N362 glycan, which is absent from CH505, and highlights light-chain residues that may alter local loop topology or charge.
c, AlphaFold3 models comparing CH103.min light-chain residues near the gp120 V5 region of JRFL and CH505wk4.c Env. The close-up highlights LC W52 and the longer JRFL V5 loop, suggesting a potential structural basis for isolate-dependent neutralization by minimally mutated CH103 variants.
d, Correlation between CH505.N197D neutralization and binding to CH505.N197D mEnv or CH505 gp120-core. Analyses include CH103.min antibodies and five antibodies recovered by single-cell sequencing or heavy/light-chain repertoire pairing (H17L8, H8L8, 10X-32, 10X-34, and sc-3). Correlations were evaluated by linear regression of log-transformed EC_{50} and IC_{50} values, with Pearson and Spearman two-tailed correlation analyses; statistics are shown in the panels.
e, Neutralization activity of CH103.mat CDRH3 mutants containing substitutions in residues encoded by putative N additions, D gene or JH6 gene segments. IC_{50} values were calculated from an assay performed in duplicate.
f, Binding of germline or UCA versions of CD4bs bnAbs CH103, VRC13 and CH235, and a partially germline-reverted VRC16 variant, to selected crosslinked mEnvs or CH505 gp120-core proteins measured by lectin-capture ELISA. Curves are from a representative experiment.

EXTENDED DATA

Extended Data Figure 1.



Extended Data Fig. 1 | Glycosylation analysis of mEnv immunogens used in this study. **a**, Site-specific glycan analysis of CH505.TF and CH505.N197D mEnv and CH505.N197D.SOS soluble Env. Glycan compositions are grouped as high-mannose, including oligomannose and hybrid-type glycans, complex-type glycans or unoccupied sites. Unresolved sites are denoted not determined (n.d.), and sites absent from a given sample are denoted not present (n.p.). Sites are numbered according to HXB2. Related data are provided in **Supplementary Table 1**. **b**, Site-specific glycan analysis of JRFL.TD15 and ADA.CM mEnv, displayed as in **a**.

Extended Data Table1. Neutralization of a HIV-1 CH505.TF mutant panel by CH103.

	CH505 mutant	IC_{50} (μg/ml)		
		CH103 UCA	CH103 Mature	Non-nAb Cocktail [1]
N-glycosylation site knock-out mutations	TF	>50	0.21	>100
	N197D	5.2	0.0021	>100
	N276D	>50	0.16	>100
	N301A	>50	0.047	>100
	N332A	>50	0.37	>100
	N386A	>50	0.12	>100
	N392A	>50	0.17	>100
	N461G	>50	0.23	>100
N197 mutations	N197E	3.79	0.0016	>100
	N197H	0.99	0.00017	>100
	N197K	1.07	0.00085	>100
	N197A	0.66	<0.0032	>100
	N197Q	>50	1.94	>100
	N197Y	*	*	*
	S199A	>50	0.75	>100
	S199P	*	*	*
Mutations reported from CH505 natural infection	R192K.N197D	1.10	0.00028	>100
	N279D	>50	0.14	>100
	N197D.N279D	1.78	0.00036	>100
	N280D	>50	0.029	>100
	N197D.N280D	40.76	0.0012	>100
	V281A	>50	0.028	>100
	N197D.V281A	0.12	0.00013	>100
	V281D	>50	0.066	>100
	N197D.V281D	0.20	0.0021	>100
	N279D.V281A	>50	0.033	>100
	N197D.N279D.V281A	0.13	0.00015	>100
	N279K	>50	0.15	>100
	G458Y	>50	1.18	>100
	N197D.N279K	24.6	0.00076	>100
	N197D.N279K ($GnTI^-$) [2]	16.5	0.0017	>100
	N197D.G458Y	>50	0.0012	>100
	N197D.G458Y ($GnTI^-$)	>50	0.0012	>100
	N197D.N279K.G458Y	>50	0.00094	>100
	N197D.N279K.G458Y ($GnTI^-$)	>50	0.00026	>100
	V5(DT) [3]	>50	2.05	>100
	N197D.V5(DT)	>50	0.011	>100
Glycosylation modified virus	TF (Kif) [4]	>50	0.52	>100
	TF (Swain) [5]	>50	0.38	>100
	TF (2FG) [6]	>50	0.17	>100
	TF (Swain+2FG)	>50	0.28	>100
	TF (GnTI-)	>50	0.35	>100
	N197D (Kif)	7.9	0.00075	>100
	N197D (Swain)	8.1	0.0013	>100
	N197D (2FG)	5.5	0.00050	>100
	N197D (Swain+2FG)	5.4	0.00048	>100
	N197D (GnTI-)	1.1	0.00082	>100

* Not infectious

[1] Non-nAb cocktail = b6, F105, HGN194, and 19b, 25 μg/ml each.

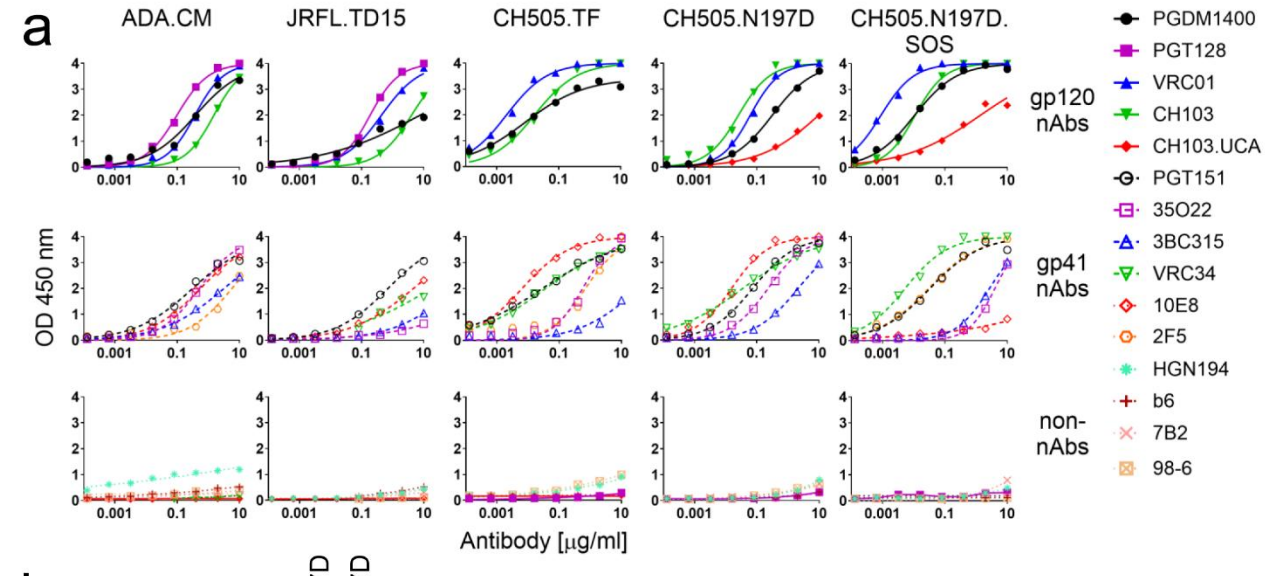
[2] GnTI-, pseudotyped virus was prepared in HEK293T cells containing a mutation in the MGAT1 gene that results in N-linked glycosylation enriched for Man5.

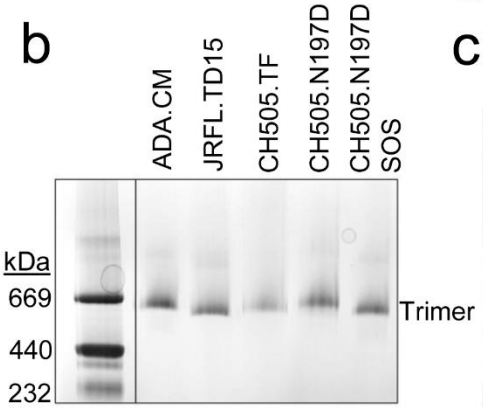
[3] V5(DT), residues DT were inserted between positions 465 and 466 in V5.

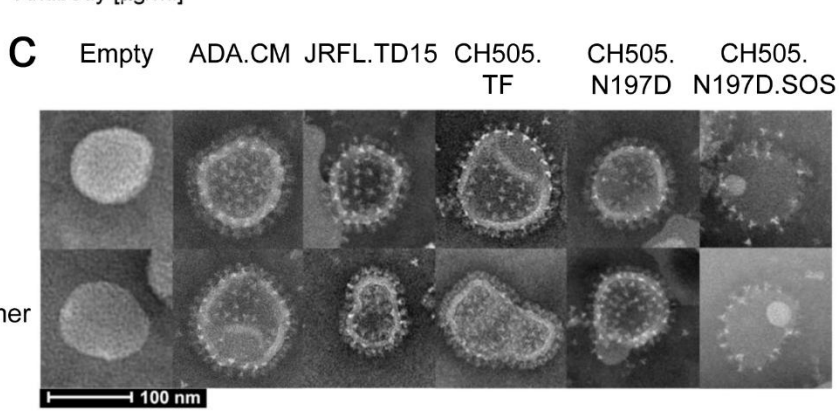
[4] Producer cells treated with kifunensine.

[5] Producer cells treated with swainsonine.
[6] Producer cells treated with 2-deoxy-2-fluoro-d-galactose.

Extended Data Figure 2.

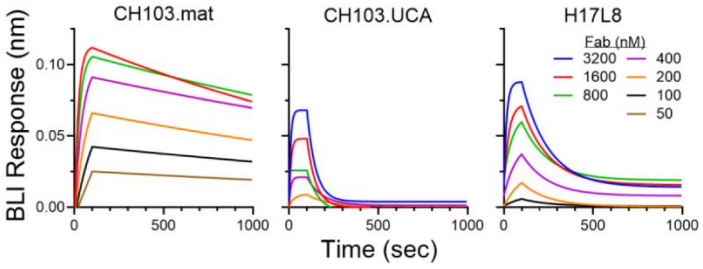






d

		gp120 core	mEnv	
		CH505	CH505 N197D.m11	JRFL.TD15
CH103. mat	KD (nM)	25.7	11.1	10.3
	kon (1/Ms)	6.80E+04	3.33E+04	2.63E+04
	kdis (1/s)	1.75E-03	3.69E-04	2.70E-04
CH103. UCA	KD (nM)	319	268	no binding
	kon (1/Ms)	2.72E+04	7.20E+04	no binding
	kdis (1/s)	8.67E-03	1.93E-02	no binding
H17L8	KD (nM)	no binding	363	20.3
	kon (1/Ms)	no binding	1.85E+04	7.44E+04
	kdis (1/s)	no binding	6.72E-03	5.55E-04



Extended Data Fig. 2 | Binding properties and physical characterization of HIV mEnv immunogens.

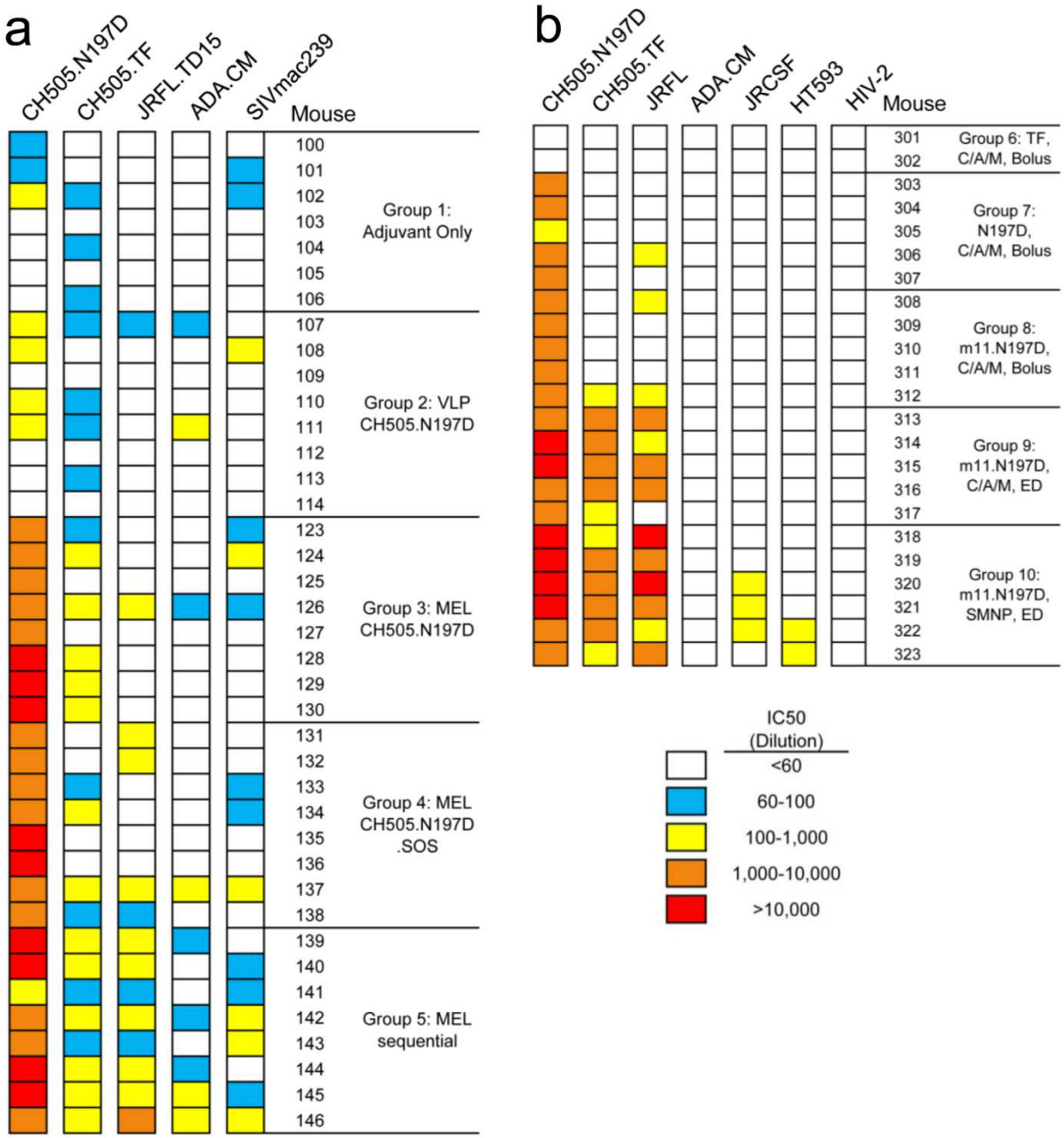
a, Binding of purified mEnv trimers to a panel of HIV-1 bnAbs and non-neutralizing antibodies measured by ELISA. Curves are from one representative experiment.

b, Blue-native PAGE analysis of purified mEnv trimers visualized by Coomassie staining.

c, Negative-stain EM images of empty liposomes and membrane Env liposomes (MELs). Empty liposomes are shown in the leftmost images.

d, Biolayer interferometry analysis of CH103.mat, CH103.UCA and H17L8 binding to CH505 gp120-core and to CH505.N197D.m11 and JRFL.TD15 mEnv. Equilibrium dissociation constants (K_D), association rates (k_{on}), dissociation rates (k_{dis}) and representative binding traces for CH505.N197D.m11 mEnv are shown.

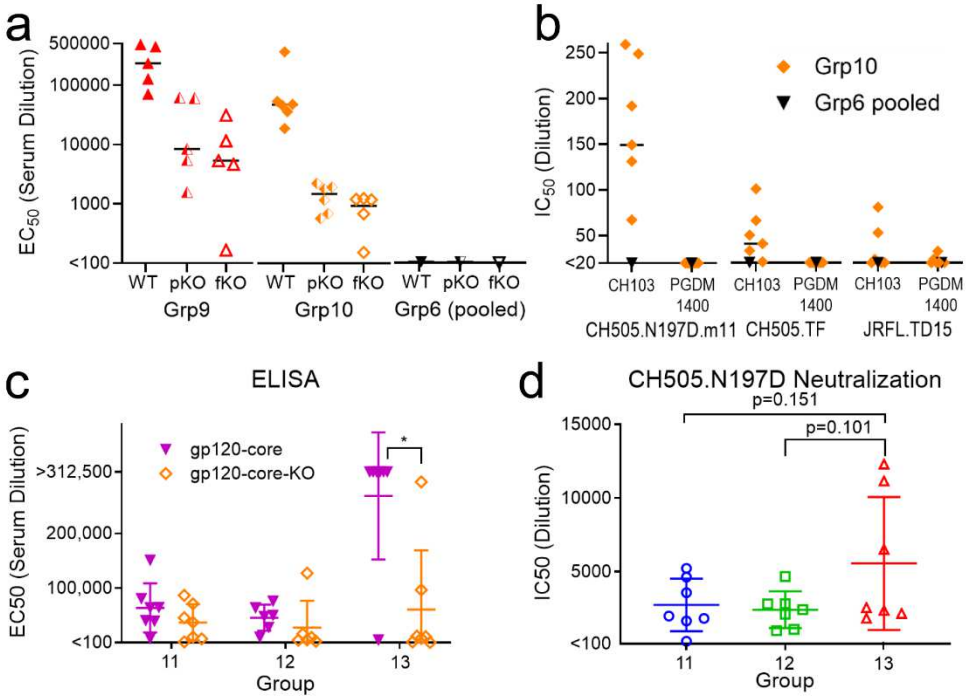
Extended Data Figure 3.



Extended Data Fig. 3 | Serum neutralization profiles from MEL01 and MEL03 immunization studies.

a,**b**, Heat maps showing serum neutralization titers, reported as IC_{50} values, for all mice in the MEL01 (**a**) and MEL03 (**b**) studies against HIV-1 isolates and the negative-control viruses HIV-2 7312A or SIVmac239. Sera in **a** were not tested below a 1:100 dilution; white therefore denotes IC_{50} <100. IC_{50} values were calculated from a single experiment performed in triplicate.

Extended Data Figure 4.



Extended Data Fig. 4 | CH505.N197D.m11 MELs with SMNP adjuvant enhance binding and neutralizing antibody responses.

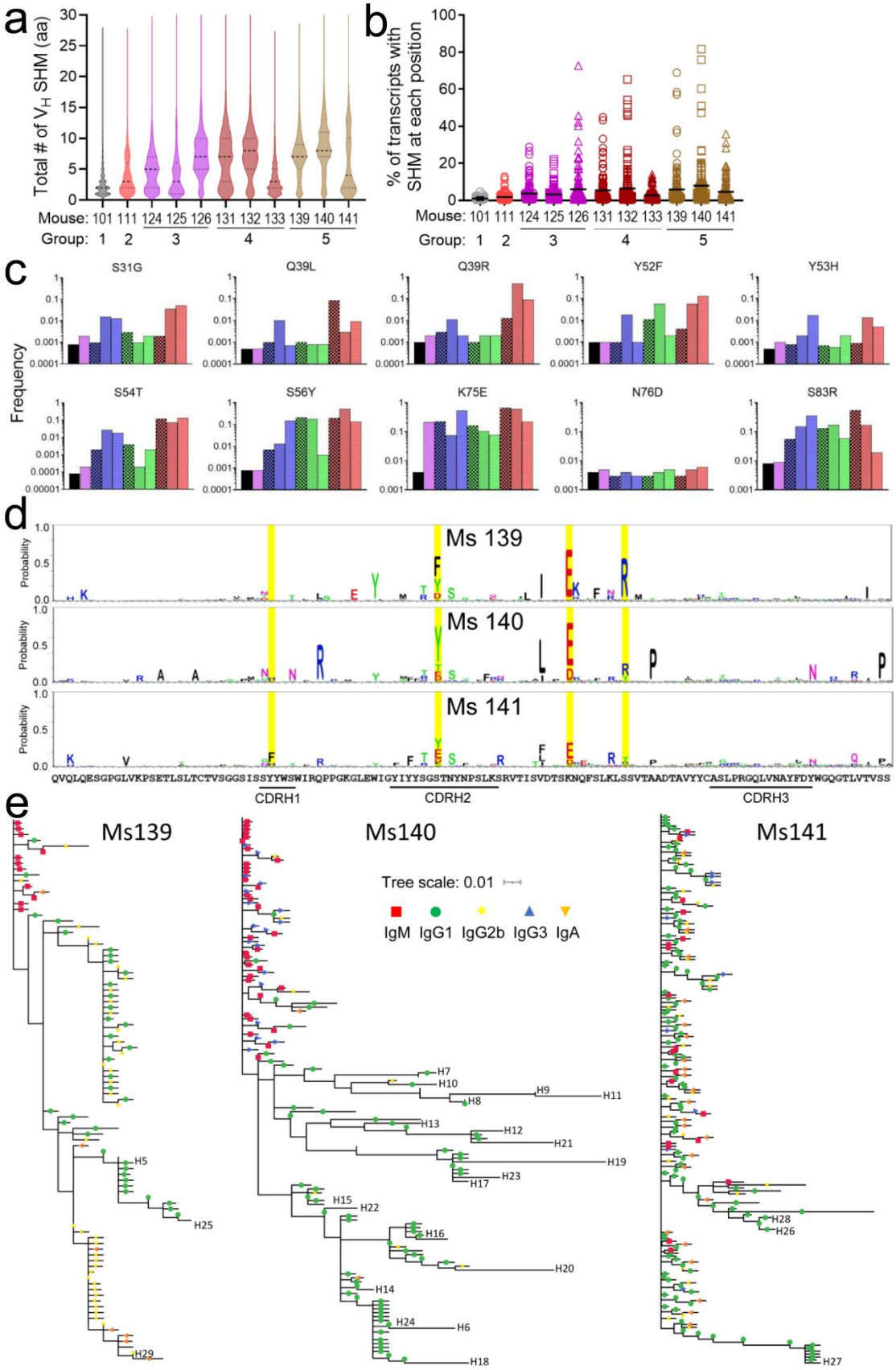
a, Sera from tier 2 cross-neutralizing Groups 9 and 10, as well as non-neutralizing Group 6 (see Fig. 2d), were tested in ELISA for binding to CH505.gp120-core.WT, partial-KO (pKO; S365K, T455E, G459E) that abolishes CH103.mat binding, and full-KO (fKO; D368R, E370A) that disrupts binding by most known CD4bs antibodies. Immunization regimens were as follows: Group 6-CH505.TF MEL, bolus injection, C/A/M adjuvant; Group 9-CH505.N197D.m11 MEL, ED prime, C/A/M adjuvant; Group 10-CH505.N197D.m11 MEL, ED prime, SMNP adjuvant.

b, Sera from MEL03 Groups 6 and 10 were tested in ELISA for the ability to block CH103 and PGDM1400 binding to mEnvs CH505.N197D.m11, CH505.TF, or JRFL.TD15 in a competition ELISA.

c, Binding by serum IgG harvested post-prime from mice in study MEL04 to CH505.gp120-core and core-pKO containing mutations that disrupt CH103.mat recognition, measured by ELISA. Groups are defined in Fig. 2h. EC_{50} values were calculated from two independent experiments. Each point represents one mouse; bars indicate median. Immunization regimens were as follows: Group 11- CH505.N197D.m11 MEL, ED prime, C/A/M adjuvant; Group 12-CH505.N197D MEL, ED prime, SMNP adjuvant; Group 13-CH505.N197D.m11 MEL, ED prime, SMNP adjuvant. Statistical significance was determined using a paired t test on log-transformed values.

d, Neutralization activity of MEL04 mouse sera against CH505.N197D virus. IC_{50} values were calculated from an experiment performed in duplicate. Each point represents one mouse; bars indicate median. P values were calculated by Kruskal–Wallis test with Dunn's correction.

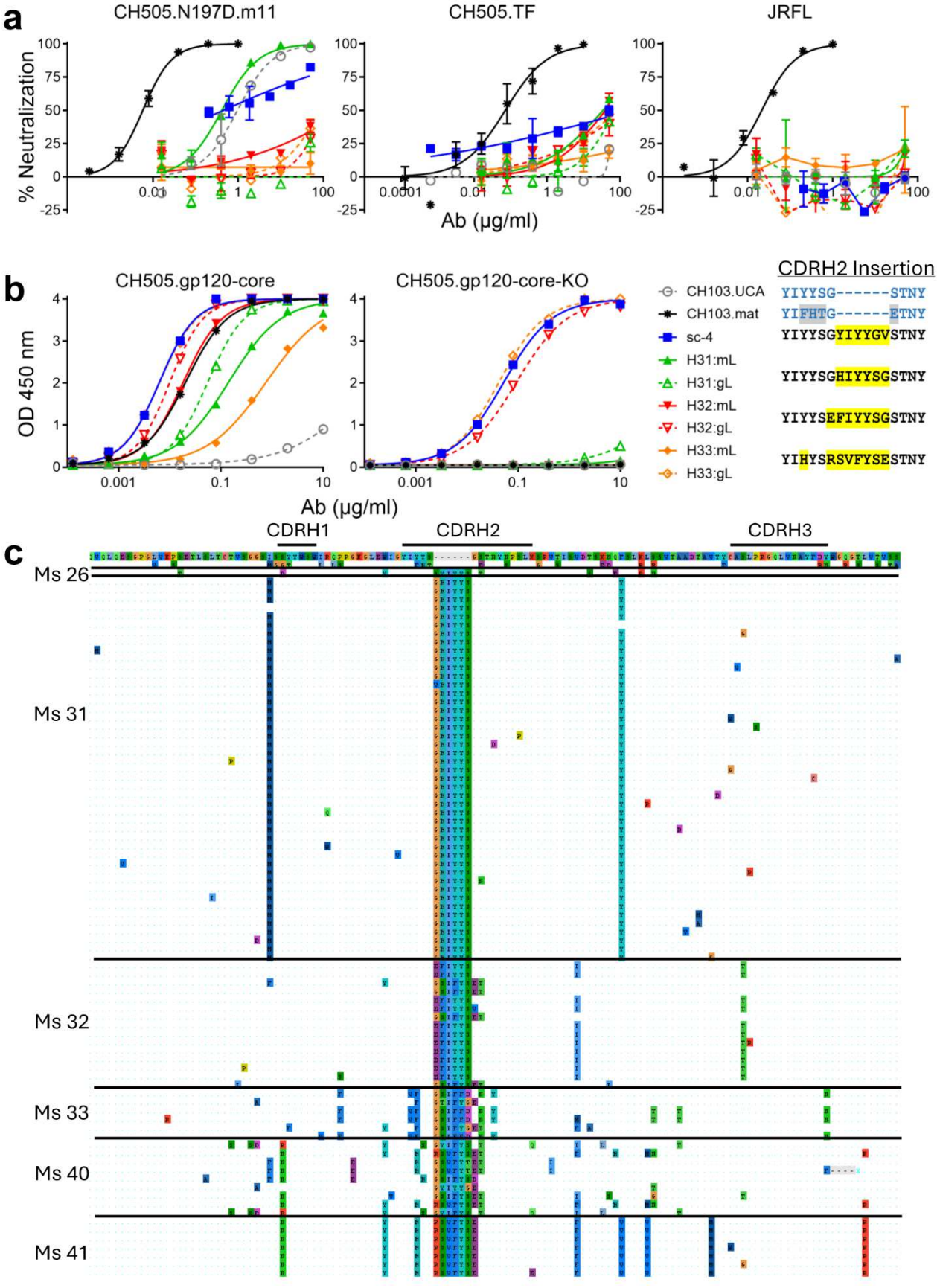
Extended Data Figure 5.



Extended Data Fig. 5 | Ig repertoire sequencing of MEL01 splenocytes reveals the distribution of CH103-lineage SHM.

a, Violin plots showing the number of amino-acid substitutions in the V_H region of CH103-lineage sequences from individual mice in MEL01 Groups 1–5.
b, Frequency of SHM at each V_H amino-acid position in CH103-lineage sequences from individual mice. Each point represents one VH position.
c, Frequencies of mature CH103-identical heavy-chain SHM associated with neutralizing activity in CH103-lineage sequences from individual MEL01 mice.
d, Sequence logo plots showing SHM frequencies in elicited CH103-lineage heavy chains from bulk Ig transcript repertoire sequencing of selected MEL01 mice. Germline-encoded amino acids are omitted to emphasize acquired substitutions; letter height indicates mutation frequency. Gp120-contact positions 32, 56, 75 and 83 are highlighted in yellow.
e, Phylogenetic trees modelling CH103.UCA-lineage diversification in individual mice and indicating antibody isotype. In collapsed trees, leaf nodes denote IgM, IgG1, IgG2b, IgG3 or IgA sequences, as indicated by the symbol key. Heavy chains selected for synthesis are labeled. Scale bar, 0.01 substitutions per site.

Extended Data Figure 6.



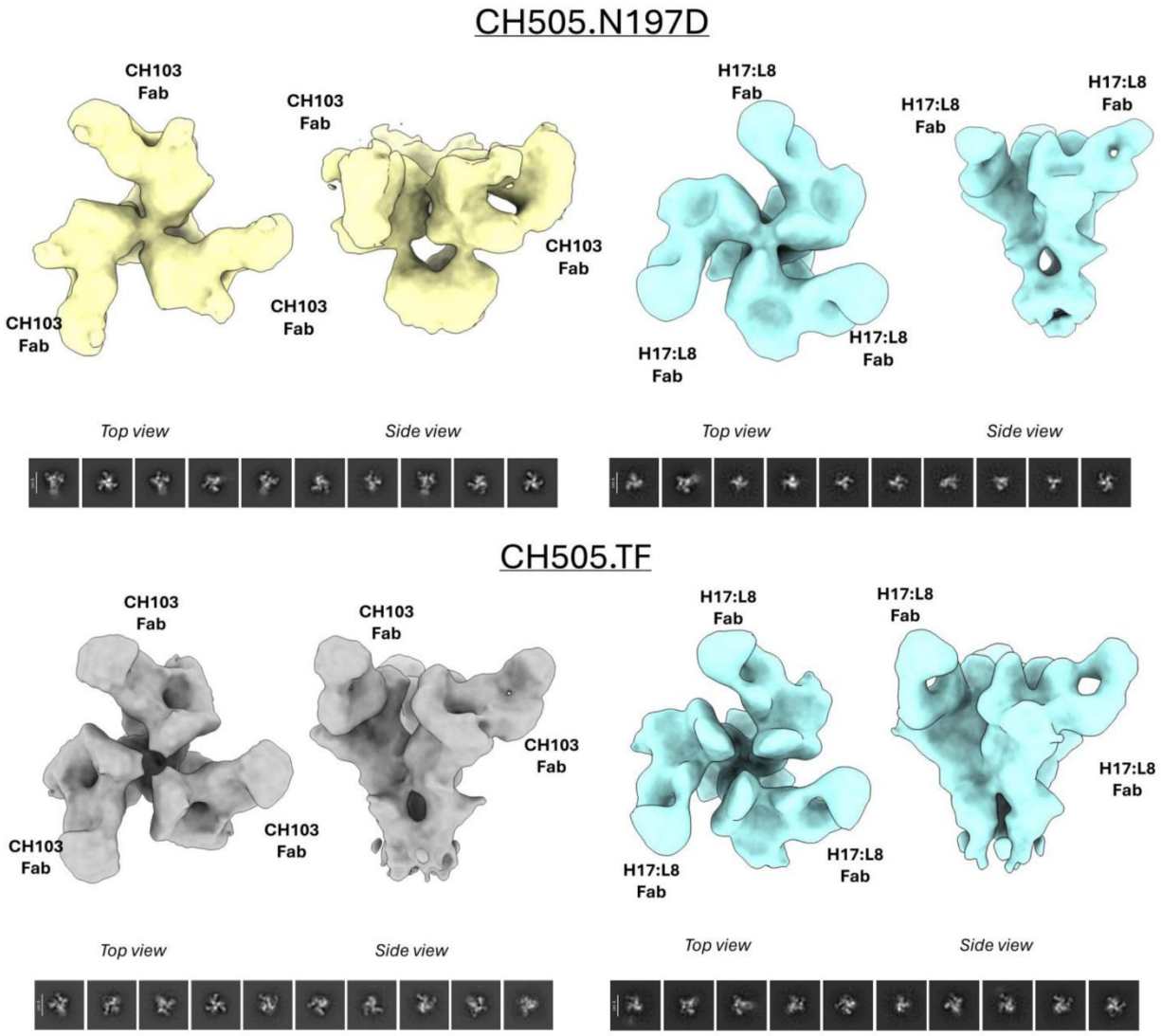
Extended Data Fig. 6 | MEL immunization elicits recurrent CH103-lineage CDRH2 insertion variants with strong CH505 gp120-core binding activity.

a, Antibody sc-4, a CH103 lineage antibody isolated by single B cell sorting, as well as H31-33, representative HC sequences identified from Ig repertoire NGS and paired with either CH103.mat or UCA LC, were tested in a neutralization assay against sensitive HIV-1 isolates. Representative assay performed in duplicate is shown. The legend is shared with panel b.

b, Antibodies with CDRH2 insertions were assessed for binding to CH505.gp120-core and its pKO version in an ELISA. Representative assay performed in duplicate is shown. The location of the insertion in the CDRH2 is shown relative to CH103 UCA and mat sequences.

c, Full V_H amino acid sequences are shown of all genes identified from Ig repertoire NGS that contained similar insertions. The top sequence is CH103.UCA and the second sequence is CH103.mat. Differences from CH103.UCA sequence are highlighted.

Extended Data Figure 7.



Extended Data Fig. 7 | Negative-stain EM three-dimensional reconstructions of CH103 antibodies bound to Env.

Negative-stain EM three-dimensional reconstructions of CH103.mat and H17L8 Fab complexes with CH505.TF and CH505.N197D membrane Env showing recognition of trimeric mEnv in a binding mode consistent with the cryo-EM structures. The inset images below each reconstruction show representative 2D class averages.

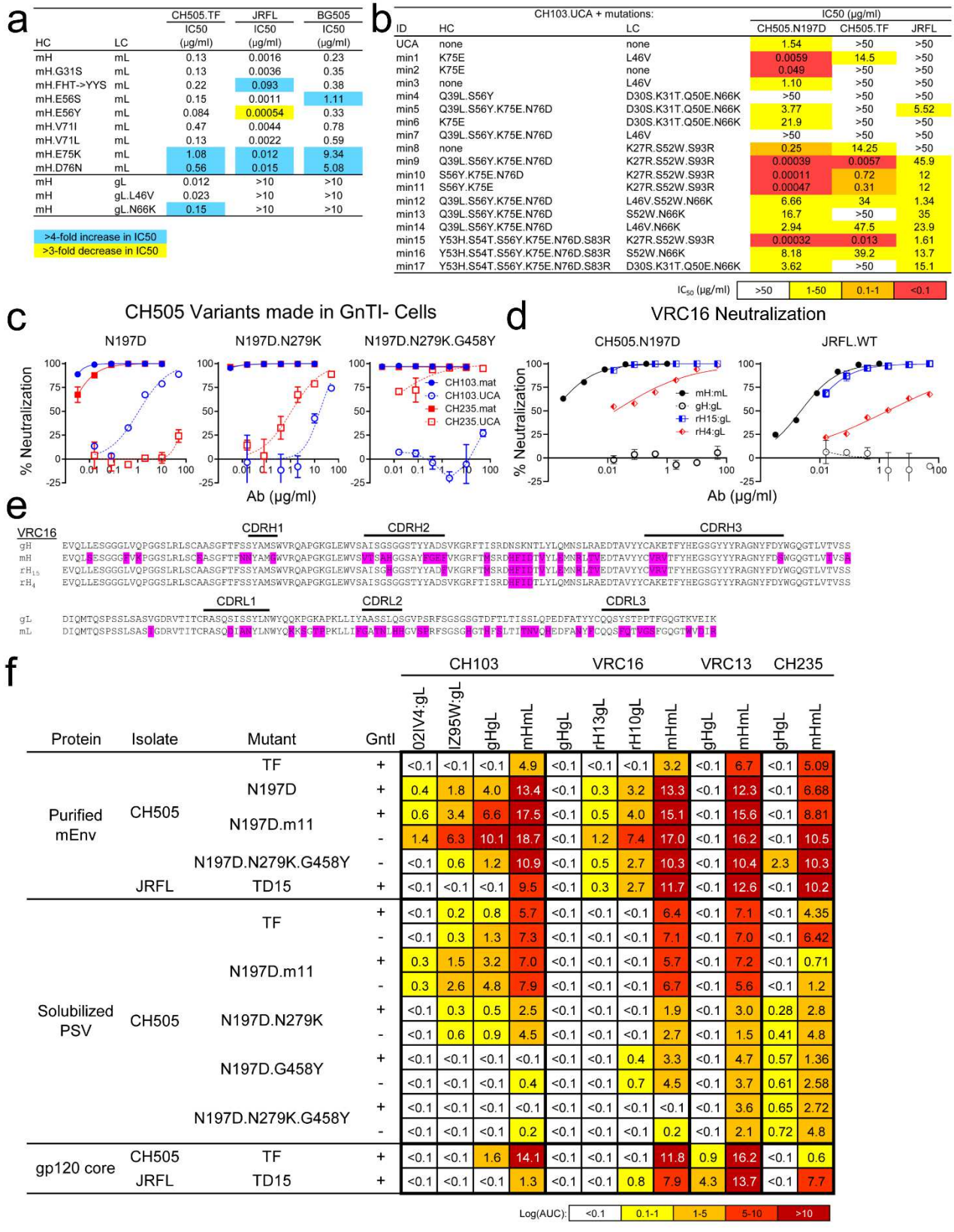
Extended Data Table 2. CH103.mat and H17L8 contact residues in cryo-EM models.

Chain	Residue	CH505wk4.c Contact(s)	Adjacent gp120	UCA or SHM	Buried Surface Area (Å^2)
H	Y33	G367, D368	x	UCA	30
H	Y50	G367	x	UCA	18
H	F52	D368, Q428	x	SHM	19
H	H53	N195, Q428, V430	x	SHM	72
H	T54	I194, N195, N425	x	SHM	62
H	G55	I194, N195, N425	x	UCA	33
H	E56	I194, D368, L369	x	SHM	69
H	S70	N197NAG	x	UCA	28
H	V71	N195, T198	x	UCA	21
H	D72	T198	W316	UCA	38
H	T73	T198, V430	x	UCA	53
H	S74	X	G314, W316	UCA	54
H	E75	X	W316, Y318	SHM	82
H	D76	X	K207	SHM	25
H	R82a	D185, G186	x	SHM	53
H	R97	D368, Q428	x	UCA	107
H	G98	V371	x	UCA	27
H	Q99	S365, T455	x	UCA	118
H	L100	S365, G366, G367	x	UCA	28
H	V100a	S365, D457, R469	x	UCA	58
H	N100b	N280, D457	x	UCA	47
L	N32	G458	x	SHM	45
L	E50	N280	x	SHM	29
L	N51	G459	x	SHM	22
L	K53	N280	x	UCA	23
L	K66	G459, K460	x	SHM	24
L	W91	S365, G366, R469	x	UCA	79
L	F94	N386NAG, N386BMA	x	UCA	114

Chain	Residue	JRFL.TD15 Contact(s)	Adjacent gp120	UCA or SHM	Buried Surface Area (Å^2)
H	I29	V430	x	UCA	17
H	S30	Q428	x	UCA	38
H	N31	Q428	x	SHM	16
H	Y33	G367, D368	x	UCA	30
H	Y52	D368, Q428	x	UCA	19
H	Y53	N425, Q428, V430	x	UCA	86
H	S54	I194, N425	x	UCA	65
H	G55	I194	x	UCA	29
H	Y56	I194, G367, P369	x	SHM	71
H	S65	N186	x	UCA	19
H	I71	T198	x	SHM	17
H	D72	T198	R308	UCA	50
H	P73	T198, V430	x	SHM	38
H	S74	T198	G314	UCA	56
H	E75	x	Y318	SHM	71
H	D76	x	K207	SHM	22
H	R82a	D185, N186	x	SHM	63
H	R97	D368, I371, Q428	x	UCA	103
H	G98	I371	x	UCA	23

H	Q99	S365, I371, T455	x	UCA	108
H	L100	S365, G366, G367	x	UCA	35
H	V100a	S365, D457, R469	x	UCA	61
H	N100b	D457	x	UCA	58
L	R27	N362NAG	x	SHM	42
L	D30	N362NAG	x	UCA	77
L	Y32	D457, G459	x	UCA	100
L	Q50	N280, G459	x	UCA	49
L	D51	I460	x	UCA	19
L	W52	G458, I460, N276NAG	x	SHM	68
L	K53	N280	x	UCA	30
L	K66	I460	x	SHM	35
L	W91	S365	x	UCA	30
L	R93	H363, N386NAG	x	SHM	91
L	F94	N386NAG, N386BMA	x	UCA	117

Extended Data Figure 8.



a		CH505.TF	JRFL	BG505
		IC50	IC50	IC50
HC	LC	(μg/ml)	(μg/ml)	(μg/ml)
mH	mL	0.13	0.0016	0.23
mH.G31S	mL	0.13	0.0036	0.35
mH.FHT->YYS	mL	0.22	0.093	0.38
mH.E56S	mL	0.15	0.0011	1.11
mH.E56Y	mL	0.084	0.00054	0.33
mH.V71I	mL	0.47	0.0044	0.78
mH.V71L	mL	0.13	0.0022	0.59
mH.E75K	mL	1.08	0.012	9.34
mH.D76N	mL	0.56	0.015	5.08
mH	gL	0.012	>10	>10
mH	gL.L46V	0.023	>10	>10
mH	gL.N66K	0.15	>10	>10

>4-fold increase in IC50
>3-fold decrease in IC50

b	CH103.UCA + mutations:		IC50 (μg/ml)		
ID	HC	LC	CH505.N197D	CH505.TF	JRFL
UCA	none	none	1.54	>50	>50
min1	K75E	L46V	0.0059	14.5	>50
min2	K75E	none	0.049	>50	>50
min3	none	L46V	1.10	>50	>50
min4	Q39L.S56Y	D30S.K31T.Q50E.N66K	>50	>50	>50
min5	Q39L.S56Y.K75E.N76D	D30S.K31T.Q50E.N66K	3.77	>50	5.52
min6	K75E	D30S.K31T.Q50E.N66K	21.9	>50	>50
min7	Q39L.S56Y.K75E.N76D	L46V	>50	>50	>50
min8	none	K27R.S52W.S93R	0.25	14.25	>50
min9	Q39L.S56Y.K75E.N76D	K27R.S52W.S93R	0.00039	0.0057	45.9
min10	S56Y.K75E.N76D	K27R.S52W.S93R	0.00011	0.72	12
min11	S56Y.K75E	K27R.S52W.S93R	0.00047	0.31	12
min12	Q39L.S56Y.K75E.N76D	L46V.S52W.N66K	6.66	34	1.34
min13	Q39L.S56Y.K75E.N76D	S52W.N66K	16.7	>50	35
min14	Q39L.S56Y.K75E.N76D	L46V.N66K	2.94	47.5	23.9
min15	Y53H.S54T.S56Y.K75E.N76D.S83R	K27R.S52W.S93R	0.00032	0.013	1.61
min16	Y53H.S54T.S56Y.K75E.N76D.S83R	S52W.N66K	8.18	39.2	13.7
min17	Y53H.S54T.S56Y.K75E.N76D.S83R	D30S.K31T.Q50E.N66K	3.62	>50	15.1

IC_{50} (μg/ml): >50 | 1-50 | 0.1-1 | <0.1

f				CH103				VRC16			VRC13		CH235	
Protein	Isolate	Mutant	GntI	02IV4:gL	IZ95W:gL	gHgL	mHmL	gHgL	rH13gL	rH10gL	mHmL	gHgL	mHmL	gHgL	mHmL
Purified mEnv	CH505	TF	+	<0.1	<0.1	<0.1	4.9	<0.1	<0.1	<0.1	3.2	<0.1	6.7	<0.1	5.09
		N197D	+	0.4	1.8	4.0	13.4	<0.1	0.3	3.2	13.3	<0.1	12.3	<0.1	6.68
		N197D.m11	+	0.6	3.4	6.6	17.5	<0.1	0.5	4.0	15.1	<0.1	15.6	<0.1	8.81
			-	1.4	6.3	10.1	18.7	<0.1	1.2	7.4	17.0	<0.1	16.2	<0.1	10.5
		N197D.N279K.G458Y	-	<0.1	0.6	1.2	10.9	<0.1	0.5	2.7	10.3	<0.1	10.4	2.3	10.3
	JRFL	TD15	+	<0.1	<0.1	<0.1	9.5	<0.1	0.3	2.7	11.7	<0.1	12.6	<0.1	10.2
Solubilized PSV	CH505	TF	+	<0.1	0.2	0.8	5.7	<0.1	<0.1	<0.1	6.4	<0.1	7.1	<0.1	4.35
			-	<0.1	0.3	1.3	7.3	<0.1	<0.1	<0.1	7.1	<0.1	7.0	<0.1	6.42
		N197D.m11	+	0.3	1.5	3.2	7.0	<0.1	<0.1	<0.1	5.7	<0.1	7.2	<0.1	0.71
			-	0.3	2.6	4.8	7.9	<0.1	<0.1	<0.1	6.7	<0.1	5.6	<0.1	1.2
		N197D.N279K	+	<0.1	0.3	0.5	2.5	<0.1	<0.1	<0.1	1.9	<0.1	3.0	0.28	2.8
			-	<0.1	0.6	0.9	4.5	<0.1	<0.1	<0.1	2.7	<0.1	1.5	0.41	4.8
		N197D.G458Y	+	<0.1	<0.1	<0.1	<0.1	<0.1	<0.1	0.4	3.3	<0.1	4.7	0.57	1.36
			-	<0.1	<0.1	<0.1	0.4	<0.1	<0.1	0.7	4.5	<0.1	3.7	0.61	2.58
		N197D.N279K.G458Y	+	<0.1	<0.1	<0.1	<0.1	<0.1	<0.1	<0.1	<0.1	<0.1	3.6	0.65	2.72
			-	<0.1	<0.1	<0.1	0.2	<0.1	<0.1	<0.1	0.2	<0.1	2.1	0.72	4.8
gp120 core	CH505	TF	+	<0.1	<0.1	1.6	14.1	<0.1	<0.1	<0.1	11.8	0.9	16.2	<0.1	0.6
	JRFL	TD15	+	<0.1	<0.1	<0.1	1.3	<0.1	<0.1	0.8	7.9	4.3	13.7	<0.1	7.7

Log(AUC): <0.1 | 0.1-1 | 1-5 | 5-10 | >10

Extended Data Fig. 8 | Germline-reverted CD4bs antibodies recognize related CH505 Env variants.

a, Neutralization activity of CH103 variants carrying point mutations selected from Ig repertoire sequencing and structural analyses. Heavy-chain mutations were introduced into CH103.mat, whereas light-chain mutations were introduced into CH103.mHgL. Antibodies were tested against CH505.TF, JRFL and BG505. IC_{50} values were calculated from an experiment performed in duplicate.
b, Neutralization activity of minimally mutated CH103 variants against CH505.N197D, CH505.TF and JRFL. IC_{50} values were calculated from the average of two independent experiments performed in duplicate.
c, Neutralization of CH505 point-mutant viruses produced in GnTI- cells, which enrich for Man5 N-glycosylation, by CH103.UCA, CH235.UCA and their mature counterparts. Representative assay performed in duplicate is shown.
d, Neutralization of CH505.N197D and JRFL by VRC16 heavy-chain germline revertants paired with VRC16 germline light chain. Representative assay performed in duplicate is shown.
e, Sequence alignment of VRC16 heavy-chain germline revertants with inferred germline and mature VRC16 heavy chains. SHM are highlighted in purple. Mature and germline VRC16 Vλ sequences are shown below.
f, Binding of CD4bs bnAbs and their germline or UCA counterparts to purified GA-crosslinked mEnv, detergent-solubilized CH505 mutant viral supernatants produced in 293T or GnTI- cells, and gp120-core proteins, measured by lectin-capture ELISA. CH103.UCA heavy-chain homologues IZ95W and 01IV4, and partially germline-reverted VRC16 variants rH15 and rH4, are also included. Values indicate the area under the curve from ELISA titrations beginning at 10 μg/ml.

Supplementary Files

This is a list of supplementary files associated with this preprint. Click to download.

- SupplementNatCommCH103RevisionFinal.docx